

Infrared Light Curves of Mira Variable Stars from COBE DIRBE Data

Beverly J. Smith

*Department of Physics and Astronomy, East Tennessee State University, Box 70652, Johnson City, TN
37614*

smithbj@etsu.edu

David Leisawitz

Goddard Space Flight Center

leisawitz@stars.gsfc.nasa.gov

Michael W. Castelaz

Pisgah Astronomical Research Institute, 1 PARI Drive, Rosman, NC 28772

mcastelaz@pari.edu

Donald Luttermoser

*Department of Physics and Astronomy, East Tennessee State University, Box 70652, Johnson City, TN
37614*

lutter@etsu.edu

ABSTRACT

We have used the COBE DIRBE database to derive near- and mid-infrared light curves for a well-defined sample of 38 infrared-bright Mira variable stars, and compared with optical data from the AAVSO. In general, the $3.5\ \mu\text{m}$ and $4.9\ \mu\text{m}$ DIRBE bandpasses provide the best S/N light curves, with S/N decreasing with wavelength at longer wavelengths. At $25\ \mu\text{m}$, good light curves are only available for $\sim 10\%$ of our stars, and at wavelengths $\geq 60\ \mu\text{m}$, extracting high quality light curves is not possible. The amplitude of variability is typically less in the near-infrared than in the optical, and less in the mid-infrared than in the near-infrared, with decreasing amplitude with increasing wavelength. On average, there are 0.20 ± 0.01 magnitudes variation at $1.25\ \mu\text{m}$ and 0.14 ± 0.01 magnitudes variation at $4.9\ \mu\text{m}$ for each magnitude variation in V. The observed amplitudes are consistent with results of recent theoretical models of circumstellar dust shells around Mira variables. For a few stars in our sample, we find clear evidence of time lags between the optical and near-infrared maxima of phase $\sim 0.05 - 0.13$, with no lags in the minima. For three stars, mid-infrared maximum appears to occur slightly before that in the near-infrared, but after optical maximum. We find three examples of secondary maxima in the rising portions of the DIRBE light curves, all of which have optical counterparts in the AAVSO data, supporting the hypothesis that they are due to shocks rather than newly-formed dust layers. We find no conclusive evidence for rapid (hours to days) variations in the infrared brightnesses of these stars.

Subject headings: stars: AGB and post-AGB, stars: variable: Miras

1. Introduction

Current theories of stellar evolution indicate that low mass ($\leq 8 M_{\odot}$) stars pass through the pulsating Mira star phase at the end of their time as Asymptotic Giant Branch stars (Wood 1997; Olofsson 1999). Although the time that stars spend as Mira variables is relatively short ($\sim 6 \times 10^4$ years; Wood (1990)), this stage is very important because these stars have very high rates of mass loss (up to $10^{-4} M_{\odot} \text{ yr}^{-1}$; Knapp & Morris (1985)). This means that they return large quantities of carbon, oxygen, and nitrogen-enriched gas to the interstellar medium (Sedlmayr 1994). At present, the mass loss process, the properties of the circumstellar envelopes of these stars, and how these relate to the variability of the star are still not very well-understood.

To better understand these processes, detailed studies of Mira variables at infrared wavelengths are helpful. In the near-infrared, photospheric emission dominates, while at wavelengths longer than $\sim 3 \mu\text{m}$ emission from dust in the circumstellar envelope becomes important (Woolf & Ney 1969). Infrared observations have been used to constrain models of the circumstellar envelopes of Mira variables and to estimate mass loss rates from these stars (Jura 1986; Bedijn 1987; Onaka et al. 1989a,b; Anandarao et al. 1993; Le Bertre & Winters 1998). These studies, however, are based on time-averaged broadband fluxes from the Infrared Astronomical Satellite (IRAS) (Jura 1986; Bedijn 1987; Anandarao et al. 1993; Le Bertre & Winters 1998) or time-averaged $8 - 23 \mu\text{m}$ IRAS Low Resolution Spectrometer (LRS) spectra (Onaka et al. 1989a,b), and have not investigated mid- or far-infrared variability of these stars.

To better understand mass loss in these stars, infrared monitoring is helpful. Such studies have revealed variations in the infrared spectral energy distributions of Miras with time. Broadband infrared observations indicate that the amplitude of variation tends to decrease with wavelength from the optical through the mid-infrared (Lockwood & Wing 1971; Harvey et al. 1974; Catchpole et al. 1979; Barthes, Chenevez, & Mattei 1996; Le Bertre 1992, 1993; Little-Marenin et al. 1996). Spectroscopic observations with IRAS (Little-Marenin & Stencel 1992; Hron & Aringer 1994; Little-Marenin et al. 1996), ground-based

telescopes (Creech-Eakman et al. 1997; Monnier et al. 1998), and the Infrared Space Observatory (ISO) (Onaka et al. 1997) showed that at least for some Miras the silicate features tend to decrease in flux from light curve maximum to minimum. There is also evidence from IRAS data for far-infrared variations of Miras (Little-Marenin & Stencel 1992; Little-Marenin et al. 1996; Spear et al. 1993), however, the IRAS light curves are poorly-sampled, so variations at these wavelengths are not well-studied.

Infrared monitoring of Mira variables has also revealed wavelength-dependent phase lags. The maxima at $1 \mu\text{m}$ (Petit & Nicholson 1933; Lockwood & Wing 1971; Barnes 1973) and $2.7 \mu\text{m}$ (Maran et al. 1977) typically lag those at V by about 0.1 phase, while no lags are seen in the minima. At present, phase lags at longer wavelengths are not well-determined. There have also been a few reported observations of large-amplitude (0.5 – 1 magnitudes) very short-term (hours to days) variations in the visual (Maffei & Tosti 1995; de Laverny et al. 1998) and near-infrared (Smak & Wing 1979b; Guenter & Henson 2001) light curves of Mira variables, but such variations have not yet been reported at longer wavelengths.

The previously-cited studies generally provide long-wavelength infrared light curves for only a relatively small sample of stars, and generally sample only a fraction of the light curve of these stars. To obtain more complete infrared light curves for a larger sample of Mira stars, we have used data from the Diffuse Infrared Background Experiment (DIRBE) instrument (Hauser et al. 1998) on the Cosmic Background Explorer (COBE) spacecraft (Boggess et al. 1992). To date, little research has been done on infrared variability of stars using DIRBE data, in spite of its suitability for such studies.

The COBE satellite was launched in November 1989, and the DIRBE instrument functioned at cryogenic temperatures from 11 December 1989 until 21 September 1990. This 10 month timescale is suitable for searching for variations in long period variables. In the course of a week, a typical point on the sky was observed 10-15 times by DIRBE, and over the course of the cryogenic mission, it was observed about 200 times (Hauser et al. 1998). The temporal coverage of DIRBE varies with sky position. Some parts of the sky

had relatively complete coverage; for other regions, there were gaps in the coverage of several months (Hauser et al. 1998). DIRBE operated at 10 infrared wavelengths (1.25, 2.2, 3.5, 4.9, 12, 25, 60, 100, 140, and 240 μm), providing a nearly complete infrared spectrum. This allows us to tie stellar phenomena, as seen in the visual and near-infrared, to circumstellar emission, seen at longer wavelengths. The beam size of the DIRBE instrument, 0.7 degrees, although large, is still sufficiently small that individual infrared-bright stars can be discerned.

We have used DIRBE data to extract 1.25 μm – 240 μm light curves for 38 Mira variables and compared them to available optical data. We have investigated the shapes of the light curves, amplitude variations, and phase lags, and have compared these results to recent models of circumstellar dust emission from Miras.

2. Sample Selection and Infrared Light Curve Derivation

Our stars were selected from the 12 μm flux-limited sample of variable stars described by Sloan & Price (1998) and Sloan et al. (1998). This sample was obtained by cross-referencing the General Catalogue of Variable Stars (Kholopov et al. 1985-1988) with the IRAS Point Source Catalog (1988). We selected a subset of this sample, with an IRAS 12 μm flux density cutoff of 235 Jy and classification as Mira stars. A total of 38 stars are included in our set (Tables 1 and 2). Eight of these are classified as carbon-rich Mira variables (Table 1), while 30 are oxygen-rich (Table 2). In Tables 1 and 2, we provide the positions, the period of variability, the IRAS 12 μm magnitude, the optical spectral type, and the dust spectral type (based on the IRAS LRS spectra). The positions are from the SIMBAD database; the rest of the information is from Sloan & Price (1998) or Sloan et al. (1998).

Infrared light curves were derived for these stars from the DIRBE data using two methods. We first extracted light curves from the COBE DIRBE Weekly Sky Maps. These are weekly-averaged intensity maps of the sky in the ten DIRBE wavelength bands. The stellar photometry was determined by multiplying the surface brightness of the Weekly Sky Maps at the stellar position by the

DIRBE beam solid angle, after sky subtraction. For sky values, we used the average of the fluxes at four positions 2° N, S, E, and W in equatorial coordinates. Flux uncertainties were obtained by using the quoted DIRBE photometric uncertainties combined in quadrature with the dispersion in the four sky measurements. At 1.25 μm – 240 μm , respectively, the average noise levels in these light curves are 35 Jy, 40 Jy, 35 Jy, 20 Jy, 120 Jy, 155 Jy, 140 Jy, 460 Jy, 2850 Jy, and 1250 Jy.

The second method of obtaining light curves used the DIRBE Calibrated Individual Observations (CIO) data files. The CIO database contains the calibrated individual 1/8th second samples taken in science-survey mode during each day of the cryogenic mission. For all scans that passed within 0.3° of the target position, a linear baseline was fit to the sections $\pm 1.35^\circ - 2.25^\circ$ from the point of closest approach. The point source photometry was obtained by subtraction of this baseline and correcting for DIRBE beam response. The uncertainties in the point source photometry are calculated as the quadrature sum of the rms noise of the baseline, an error due to positional uncertainties of 1' in both the in-scan and cross-scan directions, an error due to short-term detector gain variations, and signal-dependent detector noise. For the light curves derived from the CIO data, average noise levels per datapoint are 25 Jy, 20 Jy, 20 Jy, 10 Jy, 30 Jy, 55 Jy, 320 Jy, 765 Jy, 4800 Jy, and 2750 Jy for the DIRBE 1.25 – 240 μm filters, respectively.

Datapoints with large uncertainties (greater than three times the average uncertainty) were eliminated from the dataset, since anomalously large errorbars were likely caused by cosmic ray hits or the presence of a nearby companion in the DIRBE scan. Careful comparison of individual DIRBE scan locations with the IRAS Point Source Catalog (1988) and the all-sky near-infrared catalog developed by Smith (1995) for position reconstruction for the Infrared Telescope in Space (IRTS) mission (Murakami et al. 1996; Wheaton et al. 1997) shows that when an infrared-bright companion was present in the baseline portion of the scan, the derived stellar photometry was sometimes discrepant with large uncertainties.

These two methods provided consistent light curves, with flux densities that agree within 15%, 4%, 12%, 2%, 6%, 3%, and 12%, for the 1.25

μm - $60 \mu\text{m}$ bands, respectively, when averaged over our light curves. As noted in the DIRBE Explanatory Supplement (Hauser et al. 1998), point source photometry from the Weekly Sky Maps may suffer a small systematic offset when compared to the CIO data. The CIO data are believed to be more accurate for point source photometry (Hauser et al. 1998), so for the following analysis we focus on the CIO light curves. Note that for the six shortest wavelengths, the uncertainties in the CIO light curves are less than those of the photometry derived from the Weekly Sky Maps, in spite of the shorter time coverage per data point. This provides a second reason for using the CIO light curves rather than the light curves from the Weekly Sky Maps.

Note that the uncertainties used in this paper do not include absolute flux calibration errors, and that color corrections were not made to the DIRBE flux densities. The color corrections are typically quite small, particularly at the shorter DIRBE wavelengths. For the stars in our sample, the color correction tables in Hauser et al. (1998) give estimated color correction factors ($F_{\text{observed}}/F_{\text{true}}$) that range from 0.99 - 1.03 at $1.25 \mu\text{m}$, 0.99 - 1.03 at $2.2 \mu\text{m}$, 0.98 - 1.01 at $3.5 \mu\text{m}$, 0.99 - 1.01 at $4.9 \mu\text{m}$, 0.89 - 1.1 at $12 \mu\text{m}$, and 0.5 - 2.8 at $25 \mu\text{m}$. The range quoted for each wavelength reflects the uncertainty associated with the shape of the emissivity law ($\epsilon \propto \nu^{1-2}$), the fact that the spectral energy distribution of each star is variable in time, and the fact that each star has a slightly different spectral energy distribution.

3. Optical Data

For the period of the COBE mission, 23 out of our 38 stars have well-sampled visual (V) light curves available from the American Association of Variable Star Observers (AAVSO) dataset (Mattei 2000). These stars are identified in the last column of Tables 1 and 2. These optical light curves are plotted along with the infrared data in Figures 1 and 2.

4. Results

4.1. Overview of the Light Curves

In Figure 1 we present plots of flux density vs. time for the six shortest wavelength DIRBE bands for six stars with relatively complete DIRBE light curves. In Figure 1, we also include the visual light curves when available, as well as the $2.2 \mu\text{m}$ to $12 \mu\text{m}$ flux ratio as a function of time. For RW Vel, which does not have optical data available, we also plot $F_{4.9 \mu\text{m}}/F_{2.2 \mu\text{m}}$ vs. time. In Figure 2, we provide $4.9 \mu\text{m}$ light curves for the remaining 31 stars in our sample, along with optical light curves when available. These same data are displayed in a different manner in Figure 3, where we plot the optical-infrared spectral energy distributions for all 38 stars at one or more times during the COBE mission vs. wavelength.

In general, the $3.5 \mu\text{m}$ and $4.9 \mu\text{m}$ light curves have the best S/N. At $3.5 \mu\text{m}$ and $4.9 \mu\text{m}$, respectively, on average the stars have 18.0 and 17.1 5σ weekly-averaged flux measurements from the Weekly Sky Maps (out of a total possible of 41 weeks). In the CIO light curves, at $3.5 \mu\text{m}$, the average number of datapoints is 490, and at $4.9 \mu\text{m}$, 500 points are available on average. Almost complete $4.9 \mu\text{m}$ light curves (≥ 30 weeks of 5σ data) are available for five stars in the sample, while 31 stars (82% of the sample) have at least 10 5σ datapoints available. Beyond $4.9 \mu\text{m}$, the S/N drops with increasing wavelength. At $12 \mu\text{m}$, for example, out of the 38 sample stars only 14 (37%) have more than ten datapoints detected at the 5σ level or better in the Weekly Maps. By $25 \mu\text{m}$, this number is down to nine stars (24%), and at the four longest DIRBE wavelengths, no stars have more than ten 5σ weekly datapoints in their Weekly Map light curves.

The stars in our sample are expected to be among the brightest in the infrared, so these statistics show the limitations of DIRBE data in studying infrared variability of unresolved sources. At $60 \mu\text{m}$ and longer wavelengths, the signal-to-noise ratio is too poor to obtain light curves using DIRBE data. At $25 \mu\text{m}$, good light curves (20 weeks at 5σ) are available for only four out of our 38 stars (11%).

4.2. Infrared Variability of our Sample Stars from DIRBE

In many of the light curves shown in Figures 1 and 2, variations are clearly apparent in the DIRBE data. Variations are also clearly evident in the spectral energy distributions plotted in Figure 3. The best wavelengths at which to observe variability are $3.5 \mu\text{m}$ and $4.9 \mu\text{m}$, where 30 and 31 stars, respectively, show $\geq 3\sigma$ variability in the Weekly Maps. At $25 \mu\text{m}$, only 3 stars vary more than 3σ in the weekly data.

As an approximation based on the general appearance of the light curves in Figure 1, when possible we fit the infrared light curves (in magnitude units) to sine functions to estimate amplitudes and dates of maxima (Table 3). Such fits were only possible for three stars in our sample: R Hor (Figure 1a), RW Vel (Figure 1b), and R Cas (Figure 1c). The rest of the light curves were too incomplete or too peculiar to be accurately fit to a sine function. Even for R Hor, RW Vel, and R Cas, these fits should be taken as approximations, since the light curves are not perfect sine functions. These fits, however, provide useful estimates of the amplitudes of variation and the JD dates of maxima as a function of wavelength (Table 3). Since we have less than a full pulsation cycle of infrared data for these stars, we were unable to obtain a good fit for the period of variability from the DIRBE data alone. We therefore fixed the period to be equal to that in the optical, and fit the DIRBE data for the amplitude and time of maximum. For R Hor and R Cas, we obtained the optical period by fitting the AAVSO data for $\text{JD} = 2447500 - 2448700$ (~ 3 pulsation cycles) to sine functions. We found periods of 416.5 days and 439.7 days for R Hor and R Cas, respectively, close to the values given in Sloan & Price (1998) (Table 2). For RW Vel, which does not have AAVSO data available for this time period, we simply used the period given in Sloan & Price (1998) of 443.1 days (Table 2).

The stars in our sample with almost complete DIRBE light curves (Figure 1) can be divided into two groups: those with approximately sinusoidal infrared light curves (R Hor, R Cas, and RW Vel), and those which show a plateau, or inflection point, in the rising portion of their light curves (R Car, T Cep, and S Cep). Note that all

three of the stars with sinusoidal light curves are oxygen-rich stars, while two stars with inflection points are oxygen-rich (R Car and T Cep) and one (S Cep) is a carbon star.

The best example of a secondary maximum is seen in the light curves of R Car (Figure 1b) at $\text{JD} \sim 2448045$ (phase ~ 0.75), where it is visible at all wavelengths between $1.25 \mu\text{m}$ and $12 \mu\text{m}$, and maybe at $25 \mu\text{m}$ as well, with a duration of ~ 40 days (Figure 1). These secondary maxima show an increase in brightness of $\sim 15 - 40\%$ relative to that expected from a sinusoidal light curve. This inflection point is also visible in the optical light curve, at a similar level (~ 0.4 magnitudes).

The lower S/N light curves of T Cep (Figure 1c) show weak inflection points at $\text{JD} \sim 2448020$ at $1.25 \mu\text{m}$, $2.2 \mu\text{m}$, $3.5 \mu\text{m}$, and $4.9 \mu\text{m}$, with a duration of ~ 90 days. S Cep (Figure 1a) has possible inflection points between $\text{JD} \sim 2447980 - 2448020$ in the four shortest wavelength DIRBE bands. In both cases, optical counterparts are indicated by the AAVSO data, with $\Delta\text{mag}(V) \sim 0.4$.

We also searched the CIO light curves for large amplitude, short-term (2 hours to 10 days) variations in brightness, but found no conclusive detections greater than 0.2 magnitudes at the 3σ level. A handful of datapoints with very discrepant fluxes were noted in the CIO light curves, however, these were always individual isolated points, with discrepant fluxes at only one wavelength, thus their anomalous fluxes are likely due to cosmic ray hits rather than stellar variations. We note that in the CIO data, the typical time between successive observations of the same star is ~ 9 hours, so these data are not particularly sensitive to extremely short variations.

4.3. Wavelength-Dependent Phase Lags

We used our light curves to search for phase lags of the maxima as a function of wavelength. Five of our stars (R Hor, R Cas, R Cen, R Aql, and R Aqr), all of which are oxygen-rich, have both optical and infrared data available near maximum light. All five stars show hints of an infrared delay relative to V.

The best example is R Hor (Figure 1a), which clearly shows a delay of the infrared relative to V at $1.25 \mu\text{m}$, $2.2 \mu\text{m}$, $3.5 \mu\text{m}$, and $4.9 \mu\text{m}$, and perhaps at $12 \mu\text{m}$ and $25 \mu\text{m}$ as well. The opti-

cal light curve peaks at $\text{JD} \sim 2447930$, while the infrared light curves are still rising until at least $\text{JD} \sim 2447960$, after which there are gaps in the DIRBE data until $\text{JD} \sim 2447990$. These gaps are followed by a decrease in the infrared brightness. This phase lag can also be seen in Figure 3d, the spectral energy distribution plots. The optical flux was brighter in the $\text{JD} 2447897$ spectrum than in the $\text{JD} 2447950$ spectrum, while the infrared fluxes were brighter at $\text{JD} 2447950$.

The existence of this lag is supported by our sinusoidal fits to the light curves (Table 3), which show that the $1.25 \mu\text{m}$ maximum followed that at V by ~ 53 days (0.13 phase) and the $2.2 \mu\text{m}$ maximum lagged V by ~ 65 days (0.16 phase). In Figure 4a, for the three stars for which we obtained sinusoidal fits to the light curves, we plot the phase lag relative to V as a function of wavelength. For RW Vel, for which we have no optical data, we assumed a $1.25 \mu\text{m}$ lag relative to V of 0.1 phase.

R Cas also shows evidence for an infrared to V time lag (Figure 1c; Figure 4). In the visible, R Cas was brightest at $\text{JD} \sim 2447930$, while the $1.25 \mu\text{m} - 25 \mu\text{m}$ emission was still increasing 10 days later, at $\text{JD} \sim 2447940$ (phase ~ 0.02), after which there is a gap in the DIRBE coverage. The best-fit sine curves (Table 3) show a $1.25 \mu\text{m}$ lag relative to V of 38 days (0.09 phase) and a $2.2 \mu\text{m}$ lag relative to V of 47 days (0.11 phase).

Our data suggest not just offsets between optical to infrared maxima, but also offsets between the DIRBE wavelengths. For two of our stars with relatively complete, high S/N DIRBE light curves, R Hor and R Cas, the shapes of the observed light curves differ from wavelength to wavelength. In particular, comparison of the $2.2 \mu\text{m}$, $4.9 \mu\text{m}$, and $12 \mu\text{m}$ light curves hint that the $4.9 \mu\text{m}$ and $12 \mu\text{m}$ maxima for these stars may have occurred before the $2.2 \mu\text{m}$ peaks (but after the optical maxima). The existence of these offsets is supported by our sinusoidal fits to the data (Table 3; Figure 4). For R Hor, the best fit maxima at $1.25 \mu\text{m}$ to $3.5 \mu\text{m}$ are at $\text{JD} = 2447993 \pm 6$ days (0.13 – 0.16 phase), while those at $4.9 \mu\text{m}$ to $25 \mu\text{m}$ were 30 – 50 days earlier (0.06 – 0.12 phase). For R Cas, the maxima at $1.25 \mu\text{m}$ to $3.5 \mu\text{m}$ occurred at $\text{JD} = 2447999 \pm 6$ (~ 0.10 phase), while the $4.9 \mu\text{m}$ to $25 \mu\text{m}$ peak is at $\text{JD} = 2447979 \pm 3$, 20 days earlier (~ 0.05 phase).

Of the stars with no optical data available, the

most complete infrared light curves are available for RW Vel (Figure 1b). For this star, the maxima at $1.25 \mu\text{m}$, $2.2 \mu\text{m}$, and $3.5 \mu\text{m}$ occurred at $\text{JD} = 2448023 \pm 9$, while the $4.9 \mu\text{m}$ maximum happened 40 days earlier (0.09 phase) (Table 3). This is also visible in the $F_{4.9 \mu\text{m}}/F_{2.2 \mu\text{m}}$ time plot (Figure 1b). Other stars with possible phase lags include R Cen, R Aqr, and R Aql, whose $1.25 \mu\text{m}$ maxima appear to lag those at V by ~ 30 days (0.05 – 0.1 phase). These are uncertain, however, because of incompleteness in the light curves.

In addition to a mid-infrared/near-infrared phase shift, there may be smaller offsets between the three near-infrared bands. In particular, note that for the three stars with sinusoidal fits to their light curves (Table 3; Figure 4), the $2.2 \mu\text{m}$ lags are always larger than those at $1.25 \mu\text{m}$ and $3.5 \mu\text{m}$. This result, however, is uncertain because these light curves are not perfect sine curves.

For six stars in our sample, there are both optical and infrared data available for a minimum in the light curve: R Cen, V Cyg, T Cep, R Lep, R Aqr, and R Car. In all of these cases, there is no evidence for a wavelength-dependent time delay. Of the six, the highest S/N data are those of R Car (Figure 1b), which provides a 3σ upper limit to the time lag relative to V for $1.25 \mu\text{m} - 25 \mu\text{m}$ of ~ 50 days (phase ~ 0.16). The data for R Lep (Figure 2a) provide a 3σ upper limit to a possible $4.9 \mu\text{m}$ to V time lag of 20 days (phase ~ 0.05), however, strong limits are not available for the other DIRBE wavelengths.

4.4. Amplitude Variations with Wavelength

Except for the phase lags noted above, in general the DIRBE light curves trace the optical light curves, but with smaller amplitudes of variation. For example, the optical brightness of R Hor dropped 4.5 magnitudes between $\text{JD} = 2448000$ and 2448160 (a factor of 63 in flux density), while the $1.25 \mu\text{m}$ flux density decreased by only a factor of 2.4 during this time (0.6 magnitudes). In general, the amplitude decreases with increasing wavelength. This is shown in Figure 4b, where the fitted amplitudes for the three stars in Table 3 are plotted as a function of wavelength.

As noted earlier, it was not possible to fit the light curves for most of our stars to an assumed si-

nusoidal variation, due to the incompleteness and peculiarities of the light curves. To investigate amplitude variations in a larger sample of stars, for the stars with near-continuous high S/N time coverage for at least 10 weeks in both the optical and DIRBE data, in Figure 5a we plot the *observed* change in the V magnitude vs. the *observed* change in the 1.25 μm magnitude over the time period for which we have near-continuous data. We emphasize that these magnitude changes generally do not represent the full range of variation for these stars: they only represent time ranges for which we have full sets of data. We have excluded time periods during which a maximum or minimum was occurring because of the possibility of phase lags. In Figure 5b, we plot $\Delta\text{mag}(V)$ against $\Delta\text{mag}(4.9 \mu\text{m})$, using the same criteria.

In Figures 5c – 5g, we plot $\Delta\text{mag}(1.25 \mu\text{m})$ vs. $\Delta\text{mag}(2.2 \mu\text{m})$, $\Delta\text{mag}(2.2 \mu\text{m})$ vs. $\Delta\text{mag}(3.5 \mu\text{m})$, $\Delta\text{mag}(3.5 \mu\text{m})$ vs. $\Delta\text{mag}(4.9 \mu\text{m})$, $\Delta\text{mag}(4.9 \mu\text{m})$ vs. $\Delta\text{mag}(12 \mu\text{m})$, and $\Delta\text{mag}(12 \mu\text{m})$ vs. $\Delta\text{mag}(25 \mu\text{m})$. The data plotted in these figures is for all stars in our sample, regardless of whether optical data are available, excluding only stars with less than 10 weeks of high S/N data. The magnitude changes were measured between the observed maxima and minima of the light curves, ignoring time periods during which no data were available. As with the Figures 5a and 5b, these magnitude changes do not necessarily represent the full range of variation for these stars; they are merely the magnitude changes observed in the DIRBE data.

Figures 5a and 5b show that, although the V magnitudes of these stars may vary by several magnitudes during the plotted time intervals, the 1.25 μm magnitudes typically only change by ~ 0.5 magnitudes, and the 4.9 μm typical vary by only ~ 0.25 magnitudes. On average, for every magnitude of variation in V, the 1.25 μm brightness varies by 0.20 ± 0.01 magnitudes and the 4.9 μm brightness varies by 0.14 ± 0.01 magnitudes. There is a slight correlation of $\Delta(1.25 \mu\text{m})$ with ΔV , and no observed correlation of $\Delta(4.9 \mu\text{m})$ with ΔV .

In all of the infrared-infrared plots (Figures 5c-5g), with the exception of $\Delta(25 \mu\text{m})$ vs. $\Delta(12 \mu\text{m})$, clear correlations are visible. The slopes of the best-fit lines are all less than one, indicating decreasing amplitude, on average, with increasing wavelength. For each magnitude

change at 1.25 μm , on average, the 2.2 μm flux changes by only 0.69 ± 0.01 magnitudes. The slope of the $\Delta\text{mag}(2.2 \mu\text{m})$ vs. $\Delta\text{mag}(3.5 \mu\text{m})$ plot is 0.83 ± 0.01 , while the best-fit $\Delta\text{mag}(3.5 \mu\text{m})$ vs. $\Delta\text{mag}(4.9 \mu\text{m})$ line has a slope of 0.96 ± 0.01 . The $\Delta\text{mag}(4.9 \mu\text{m})$ vs. $\Delta\text{mag}(12 \mu\text{m})$ best-fit line has a slope of 0.93 ± 0.04 , and the $\Delta\text{mag}(12 \mu\text{m})$ vs. $\Delta\text{mag}(25 \mu\text{m})$ slope is 0.92 ± 0.10 . Thus the decrement of the amplitude with wavelength is smaller in the mid-infrared than in the near-infrared.

In these plots, the slopes for oxygen-rich and carbon-rich stars are similar, except that oxygen-rich stars have somewhat larger $\Delta\text{mag}(2.2 \mu\text{m})/\Delta\text{mag}(1.25 \mu\text{m})$ ratios on average (0.69 ± 0.01) than the carbon-rich stars (0.39 ± 0.04), and somewhat smaller $\Delta\text{mag}(4.9 \mu\text{m})/\Delta\text{mag}(3.5 \mu\text{m})$ ratios (0.94 ± 0.01 vs. 1.26 ± 0.05). There are no significant differences between the slopes of long period (≥ 400 days) and short period stars, or between early-type (M4 – M6.5) and late-type (M7 – M10) oxygen-rich stars. The slopes for stars with dust spectral types of SE1 – SE4 are consistent with those for stars with types SE5 – SE7 (Table 2), with the exception of the $\Delta\text{mag}(12 \mu\text{m})/\Delta\text{mag}(4.9 \mu\text{m})$ ratio, which is higher in SE5 – SE7 stars (1.02 ± 0.02 vs. 0.71 ± 0.05). Spectral types SE5 – SE7 have narrower, more pronounced 9.7 μm silicate emission features than types SE1 – SE4 (Sloan & Price 1998). As noted earlier, a number of multi-epoch infrared spectroscopic studies show that, at least for some Miras, as the star increases in brightness, the strength of the silicate feature tends to increase (Little-Marenin & Stencel 1992; Hron & Aringer 1994; Little-Marenin et al. 1996; Creech-Eakman et al. 1997; Onaka et al. 1997; Monnier et al. 1998). Thus, over a pulsation period, for stars with strong silicate emission features (dust types SE5 – SE7), this effect may cause a larger change in $F_{12 \mu\text{m}}/F_{4.9 \mu\text{m}}$ than in other stars, enhancing the 12 $\mu\text{m}/4.9 \mu\text{m}$ amplitude ratios for these stars compared to stars with dust types SE1 – SE4.

Amplitude decrements with wavelength are also visible in some of the spectral energy distribution plots (Figure 3). In particular, note the variations in the spectral energy distributions of o Cet and IK Tau with time (Figures 3c and 3d). At a given wavelength, the separation between data points obtained at different times tends to get smaller as

the wavelength increases.

4.5. General Remarks about the Optical-Infrared Spectra

Figure 3 shows that the variation in the spectral energy distribution of a given star over a pulsation period is much less than star-to-star differences in spectral shape. The majority of the stars in our sample have spectral energy distributions that peak at $2.2 \mu\text{m}$, but several are brightest at $1.25 \mu\text{m}$ (for example, X Oph and R Aql; Figure 3h), and a number of stars peak at $3.5 \mu\text{m}$ (for example, R For and V Cyg; Figure 3a). Three stars, LP And (Figure 3b), V384 Per (Figure 3a), and WX Psc (Figure 3c), have very red spectral energy distributions, peaking at $4.9 \mu\text{m}$. Figure 3 shows that there is a clear statistical difference in the infrared-optical spectral energy distributions of carbon and oxygen-rich Miras, with carbon stars tending to have redder spectral energy distributions. Six of the 8 carbon stars peak at $3.5 \mu\text{m}$ or $4.9 \mu\text{m}$, but only two of the 30 oxygen stars.

We note that WX Psc, the only oxygen-rich star in our sample to peak at $4.9 \mu\text{m}$ (Figure 3c), is also the only star in our sample with an IRAS dust spectral type of ‘silicate self-absorbed emission’ (SB) (Table 2; see Sloan & Price (1998)). The rest of the stars have silicate emission spectra (dust class SE). With the exception of WX Psc, within the oxygen-rich class there is no strong correlation of the IRAS dust spectral type (Table 2) with the peak of the infrared-optical spectral energy distribution as seen in the DIRBE data (Figure 3). There is a weak correlation between optical spectral type (Table 2) and the wavelength of the peak of the optical-infrared spectrum (Figure 3), in that the two oxygen-rich stars with infrared spectral energy distributions that peak at $3.5 \mu\text{m}$ (IW Hya; Figure 3f) and $4.9 \mu\text{m}$ (WX Psc; Figure 3c) have very late optical spectral types (M9 and M8, respectively).

For the carbon-rich stars, all but two have IRAS dust spectral types of SiC, i.e., with the $11.2 \mu\text{m}$ SiC feature (Table 1, see Sloan et al. (1998)). One star (S Cep) has an IRAS spectral type of SiC+ (the $11.2 \mu\text{m}$ feature plus a secondary feature at $8.5 - 9 \mu\text{m}$). The last carbon star in our sample, LP And, has an IRAS classification of ‘red’, meaning that, in addition to the $11.2 \mu\text{m}$ feature, in the IRAS 8 – 23 μm spectrum the star shows a

strong infrared continuum increasing with increasing wavelengths. LP And is one of the two carbon stars in our sample with a very red DIRBE spectrum, peaking at $4.9 \mu\text{m}$ (Figure 3b). LP And is also the carbon star with the latest optical spectral type in our sample, C8. For the rest of the carbon stars, excluding LP And, there is no strong correlation of optical spectral type (Table 1) with DIRBE spectral peak (Figure 3).

5. Discussion

Our data show that the amplitude of variation for our sample stars decreases with increasing wavelength, from the optical out to $25 \mu\text{m}$. The amount of decrease with wavelength is consistent with the ground-based results of Le Bertre (1992, 1993). If, at a particular time during the pulsation cycle, one approximates the ratio of the fluxes in two adjacent wavelength bands by an attenuated blackbody spectrum, the observed amplitude decrease with increasing wavelength means that the temperature of this blackbody increases as the star becomes brighter.

The observed amplitude decrement with wavelength of a particular carbon-rich Mira, R For, was successfully modeled by Le Bertre (1988). In this model, the dust condensation temperature is fixed, which causes the radius of condensation to move in and out in phase with the luminosity of the star. The stellar spectrum was approximated by a blackbody, and a $\lambda^{-1.3}$ dust opacity law was used. At a given radius, the dust temperature is highest at highest stellar luminosity. Averaged over all the dust in the shell, the effective dust temperature is highest at maximum, consistent with the observations.

More general, and more complex, models for carbon-rich long period variables were developed by Winters et al. (1994b, 2000), using time-dependent hydrodynamics and a detailed treatment of the formation, growth, and evaporation of carbon grains. In these models, the pulsation of the underlying star is simulated by a sinusoidal variation of the velocity in the lowest layer of the atmosphere, and isothermal shocks and complete dust-grain momentum coupling are assumed. New layers of dust are formed periodically in the circumstellar envelope, and radiation pressure pushes this dust, and its swept-up gas, outwards. Dust

formation and growth are triggered by compression of the gas due to the pulsation, and grain nucleation, growth, and evaporation are calculated according to the relations in Gail, Keller & Sedlmayr (1984), Gail & Sedlmayr (1988), and Gauger et al. (1990). The frequency-dependent radiative transfer equation in spherical geometry is solved as in Winters, Dominik, & Sedlmayr (1994a), using gray absorption and thermal emission of the gas and frequency-dependent absorption and thermal emission of the dust. In the calculation of the dust opacity, the particles are assumed to be spherical and small compared to the relevant wavelength of the radiation field.

Using this model, Winters et al. (1994b) calculated light curves for a $1 M_{\odot}$, $10^4 L_{\odot}$ star with an assumed stellar temperature of 2600K, a period of 650 days, and a velocity amplitude of 2 km s^{-1} . They find amplitudes of 8 magnitudes at $0.55 \mu\text{m}$, 2.8 magnitudes at $0.9 \mu\text{m}$, 1 magnitude at $1.65 \mu\text{m}$, 0.7 magnitudes at $2.2 \mu\text{m}$, 0.35 magnitudes at $4.8 \mu\text{m}$, and 0.2 magnitudes at $25 \mu\text{m}$. These amplitude ratios are within a factor of two of our average values for carbon stars, with the exception of the $25 \mu\text{m}$ amplitude, which is low by a factor of four.

By comparing the DIRBE data with light curves from the AAVSO, we found evidence for time lags in the near-infrared maxima ($1.25 - 3.5 \mu\text{m}$) relative to the optical for six stars, with phase shifts between $\sim 0.05 - 0.13$. This confirms that the stellar luminosity maximum occurs after visual maximum, and the V light curve does not trace the bolometric luminosity. We also found possible lags between the near-infrared and mid-infrared maxima ($4.9 - 12 \mu\text{m}$) for three stars, with the mid-infrared flux peaking before the near-infrared but after visual maximum. The mid-infrared to near-infrared relative phase shifts are between $\sim 0.05 - 0.12$.

At present, there are no theoretical models of Miras that predict both of these lags. The well-known $1.04 \mu\text{m}$ phase lag in Miras relative to V (Lockwood & Wing 1971; Barnes 1973) has been successfully modeled by Alvarez & Plez (1998) as a consequence of the propagation of perturbations through the atmosphere. These perturbations cause time lags in the strength of the vanadium oxide absorption relative to titanium oxide, because these species are formed at different

depths in the atmosphere. The V magnitudes of M stars are strongly attenuated by TiO absorption (Smak & Wing 1979a).

Another factor that may contribute to phase lags is variations in the optical depth of the circumstellar shell, which may periodically attenuate the visual light more than the near- and mid-infrared. Extinction-induced infrared-optical offsets in the maxima are seen in the models of Winters et al. (1994b), however, in these models, optical maximum occurs after infrared maximum, while in our observations, the infrared maximum lags that in the optical. We note that the Winters et al. (1994b) models do not include the effect of molecular line opacity, while the models of Alvarez & Plez (1998) do not include dust absorption, so neither set of models do a complete analysis of phase lags. It is possible that, for some stars, dust extinction can be neglected, for example, Lobel et al. (2000) model variations in the spectral energy distribution of o Cet using the DUSTY radiative transfer code (Ivezić, Nenkova, & Elitzur 1996), and find that the circumnuclear shell of this star is optically thin. They conclude that the observed visual-to-near-infrared phase lag of Mira cannot be due to modulation of the optical by circumstellar extinction, but instead must originate in the stellar atmosphere itself.

In Section 3.2, we noted that some of our light curves are asymmetric, with secondary maxima or plateaus in the rising portion of the light curve. These two types of light curves were previously noted by Le Bertre (1992). Similar features appear in the models of Winters et al. (1994b, 1995), where they are due to the formation of a new dust layer and subsequent excess infrared dust emission. Alternative explanations for such inflection points are dissipation of shock wave energy in the inner part of the atmosphere (Feuchtinger et al. 1993) or formation of secondary shocks in the inner-most dust-free region (Bowen et al. 1990; Willson et al. 1994). The fact that matching optical excesses are present in the AAVSO data supports the hypothesis that these features are due to shocks rather than dust, since the dust models predict that extinction by the newly-formed dust layer will cause concurrent depressions (rather than enhancements) of the optical light curves.

6. Conclusions

Using data from the DIRBE instrument on COBE, we have obtained $1.25\ \mu\text{m} - 25\ \mu\text{m}$ light curves for 38 infrared-bright Mira variables and compared with AAVSO optical data. We have found decreasing amplitudes of variation with increasing wavelength, with magnitudes consistent with recent theoretical models of circumstellar dust shells around Mira stars. For the oxygen-rich Miras R Car and T Cep and the carbon star S Cep, we see secondary maxima in the rising part of the DIRBE light curves. These features are also present in the optical data from the AAVSO, suggesting that they are due to shocks rather than to dust formation.

We have detected near-infrared-to-optical time delays of the maxima of six stars with phases ~ 0.05 to 0.12 . We also find possible offsets of the mid-infrared maxima relative to those in the near-infrared for three stars, in that the mid-infrared peaks occurs after optical maximum but before that in the near-infrared. These lags may be caused by variations in the amount of molecular absorption over a pulsation period, in combination with variations in dust opacity. More detailed modeling is needed to disentangle these two effects.

We find no evidence for large magnitude (≥ 0.2 magnitudes) short-term (hours to days) variations in the near- or mid-infrared in our stars. With typical time resolution of 9 hours, however, the COBE data are not particularly sensitive to bursts of a few hours in duration.

We thank the COBE team for making this project possible. We are especially grateful to Nils Odegard, who helped developed the DIRBE CIO Point Source Photometry Research Tool, a service provided by the Astrophysics Data Facility at NASA's Goddard Space Flight Center with funding from the NSSDC. We also thank Edward Wright, whose colloquium at the University of Colorado in 1999 on the COBE mission inspired this project. We also thank two ETSU students, Mike Houchins and Randy Keeling, for help with the data acquisition. In this research, we have used, and acknowledge with thanks, data from the AAVSO International Database, based on observations submitted to the AAVSO by variable star

observers worldwide. This research has made use of the SIMBAD database, operated at CDS, Strasbourg, France. This research was funded in part by NSF POWRE grant AST-0073853.

REFERENCES

- Alvarez, R., & Plez, B. 1998, *A&A*, 330, 1109
- Anandarao, B. G., Pottasch, S. R., & Vaidya, D. B. 1993, *A&A*, 273, 570
- Barnes, T. G. 1973, *ApJS*, 25, 369
- Barthes, D., Chenevez, J., & Mattei, J. A. 1996, *AJ*, 111, 2391
- Bastian, U. & Röser, S. 1991, *Sterne und Weltraum*, 30, 592
- Bedijn, P. J. 1987, *A&A*, 186, 136
- Boggess, N. W., et al. 1992, *ApJ*, 397, 420
- Bowen, G. H. 1990, in *The Numerical Modelling of Non-linear Stellar Pulsations*, Buchler, J. R. (ed), Kluwer Academic Publishers, p. 155
- Catchpole, R. M., Robertson, B. S. C., Lloyd-Evans, T. H. H., Feast, M. W., Glass, I S., & Carter, B. S. 1979, *SAAO Circulars*, 1, 61
- Claussen, M. J., Kleinmann, S. G., Joyce, R. R., & Jura, M. 1987, *ApJS*, 65, 385
- Conrow, T., et al. 1993, *B.A.A.S.*, 183, 03.03
- Creech-Eakman, M. J., Stencel, R. E., Williams, W. J., & Klebe, D. I. 1997, *ApJ*, 477, 825
- De Laverny, P., Mennessier, M. O., Mignard, F., & Mattei, J. A. 1998, *A&A*, 330, 169
- Feuchtinger, M. U., Dorfi, E. A., & Höfner, S. 1993, *A&A*, 273, 513
- Gail, H.-P., Keller, R., & Sedlmayr, E. 1984, *A&A*, 235, 245
- Gail, H.-P., & Sedlmayr, E. 1988, *A&A*, 206, 153
- Gauger, A., Gail, H.-P., & Sedlmayr, E. 1990, *A&A*, 235, 345
- Guenter, H., & Henson, G. 2001, in preparation
- Harvey, P. M., Bechis, K. P., Wilson, W. J., & Ball, J. A. 1974, *ApJS*, 27, 331

- Hauser, M. G., Kelsall, T., Leisawitz, D., & Weiland, J. 1998, 'COBE Diffuse Infrared Background Experiment (DIRBE) Explanatory Supplement', V. 2.3.
- Hron, J. & Aringer, B. 1994, *A&A*, 281, 139
- Ivezić, Z., Nenkova, M., & Elitzur, M. 1996, User Manual for DUSTY, available on the Internet: <http://www.pa.uky.edu/moshe/dusty/>
- Ivezić, Z., & Knapp, G. R. 2000, Proceedings of IAU Symposium 191: AGB Stars, A.S.P. Conference Series, V. 203, p. 124
- IRAS Point Source Catalog (1988), Version 2, Joint IRAS Science Working Group (Washington: GPO).
- Jarrett, T. 1992, Ph.D. Thesis, University of Massachusetts.
- Jura, M. 1986, *ApJ*, 303, 327
- Knapp, G. R., Phillips, T. G., Leighton, R. B., Lo, K. Y., Wannier, P. G., Wootten, H. A., & Huggins, P. J. 1982, *ApJ*, 252, 616
- Knapp, G. R., & Morris, M. 1985, *ApJ*, 292, 640
- Koornneef, J. 1983, *A&A*, 128, 84.
- Kholopov et al. 1985-1988, General Catalog of Variable Stars.
- Le Bertre, T. 1988, *A&A*, 190, 79
- Le Bertre, T. 1992, *A&AS*, 94, 377
- Le Bertre, T. 1993, *A&AS*, 97, 729
- Le Bertre, T. 1993, *A&A*, 324, 1059
- Le Bertre, T., & Winters, J. M. 1998, *A&A*, 334, 173
- Le Sidaner, P., & Bertre, T. 1993, *A&A*, 278, 167
- Le Sidaner, P., & Bertre, T. 1996, *A&A*, 314, 896
- Little-Marenin, I. R. & Stencel, R. E. 1992, *PASPC*, 26, 591
- Little-Marenin, I. R., Stencel, R. E., & Staley, S. B. 1996, *ApJ*, 467, 806
- Lockwood, G. W. & Wing, R. F. 1971, *ApJ*, 169, 63
- Lobel, A., Bagnulo, S., Doyle, J. G., & Power, C. 2000, *MNRAS*, 317, 391
- Lobel, A., Doyle, J. G., & Bagnulo, S. 1999, *A&A*, 343, 466
- Maffei, P., & Tosti, G. 1995, *AJ*, 109, 2652
- Maran, S. P., et al. 1977, *Infrared Phys.*, 17, 565
- Mattei, J. A. 2000, Observations from the AAVSO International Database, private communication.
- Monnier, J. D., Geballe, T. R., & Danchi, W. C. 1998, *ApJ*, 502, 833
- Moshir, M., et al. 1992, Explanatory Supplement to the IRSA Faint Source Survey, Version 2, JPL D-10015 8/92 (Pasadena: JPL)
- Murakami, H., et al. 1996, *P.A.S.J.*, 48, L41
- Olofsson, H. 1999, Proceedings of the Science with the Atacama Large Millimeter Array, 45.
- Onaka, T., de Jong, T., & Willems, F. J. 1989a, *A&AS*, 81, 261
- Onaka, T., de Jong, T., & Willems, F. J. 1989b, *A&A*, 218, 169
- Onaka, T. et al. 1997, *Ap&SS*, 255, 311
- Petit, E., & Nicholson, S. B. 1933, *ApJ*, 78, 320
- Sedlmayr, E. 1994, in *Molecules in the Stellar Environment*, IAU Colloquium 146, (Springer-Verlag: New York), 163
- Skrutskie, M., et al. 1997, in *The Impact of Large-Scale Near-IR Sky Surveys*, ed. F. Garzon et al. (Dordrecht: Kluwer), 187
- Sloan, G. C., & Price, S. D. 1995, *ApJ*, 451, 758
- Sloan, G. C., & Price, S. D. 1998, *ApJS*, 119, 141
- Sloan, G. C., Little-Marenin, I. R., & Price, S. D. 1998, *AJ*, 115, 809
- Smak, J., & Wing, R. F. 1979, *Acta. Astron.*, 29, 187
- Smak, J., & Wing, R. F. 1979, *Acta. Astron.*, 29, 199

- Smith, B. J. 1995, J Band Catalog Information, Internal IPAC Memo, <http://www.etsu.edu/physics/bsmith/irtsdat/JBAND.CAT.VER5.INFO>
- Spear, G. G., Owen, B., & Madore, B. 1993, PASPC, 43, 35
- Wheaton, W. A., et al. 1997, Pointing Reconstruction Processing for IRTS, Internal IPAC Memo, <http://spider.ipac.caltech.edu/staff/waw/irts/irts.html>
- Willson, L. A., Struck-Marcell, C., & Bowen, G. H. in Cosmic Winds and the Heliosphere, eds. J. R. Jokipii, C. P. Sonett, and M. S. Giampapa
- Winters, J. M., Dominik, C., & Sedlmayr, E. 1994a, A&A, 288, 255
- Winters, J. M., Fleischer, A. J., Gauger, A., & Sedlmayr, E. 1994, A&A, 290, 623
- Winters, J. M., Fleischer, A. J., Gauger, A., & Sedlmayr, E. 1995, A&A, 302, 483
- Winters, J. M., Le Bertre, T., Jeong, K. S., Helling, C., & Sedlmayr, E. 2000, A&A, 361, 641
- Wood, P. R. 1990, in Confrontation between Stellar Pulsations and Theory, eds. C. Cacciari & G. Clementini, ASP Conf. Series 11, 355
- Wood, P. R. 1997, in Planetary Nebulae, IAU Symp. 180, 297
- Wolf, N. J., & Ney, E. P. 1969, ApJ, 155, L181

Fig. 1.— The COBE DIRBE 1.25 – 25 μm light curves from the DIRBE Weekly Maps for six sample stars with relatively complete light curves: S Cep, R Hor, RW Vel, R Car, T Cep, and R Cas. The carbon star S Cep is plotted first, followed by the five oxygen-rich stars in R.A. order. When available, optical light curves from the AAVSO are also plotted. The 12 μm /2.2 μm flux ratio as a function of time is also provided. For RW Vel, which does not have optical data available, $F_{4.9\mu\text{m}}/F_{2.2\mu\text{m}}$ is plotted instead of the optical light curve. Note that the infrared light curves are plotted in flux density units, while the optical data are given in magnitudes.

Fig. 2.— The 4.9 μm DIRBE light curves for the remaining 31 stars in our sample, from the DIRBE Weekly Maps. The carbon stars (Table 1) are plotted first, in R.A. order, followed by the oxygen-rich stars (Table 2). These are compared with optical light curves when possible.

Fig. 3.— The optical to infrared spectra for selected stars, at one to three different times during the COBE mission. The stars are plotted in R.A. order, with the carbon stars first, as in Tables 1 and 2. The symbols indicate the location in the light curve as follows: filled triangles: times near minimum; open triangles: inflection points; open circles: near infrared maximum; filled circles: optical maximum (when clearly offset from infrared maximum); open squares: times when the light curve is rising; crosses: times when the light curve is falling. A hexagon is used when it is unclear what part of the light curve the data are located. All data points within 1 day of the given time were plotted. Note that the shape of the spectra vary with time, with the shorter wavelength fluxes increasing a larger amount with increasing brightness than longer wavelength fluxes. Also note that the spectra of carbon stars tends to peak at longer wavelengths than those of oxygen-rich stars.

Fig. 4.— a) Phase lag of maximum relative to the maximum at V vs. wavelength, for the three stars with sine fits to their light curves (Table 3): R Hor (filled triangles), R Cas (open circles), and RW Vel (crosses). No appropriate optical data were available for RW Vel, so we assumed a 1.25 μm lag relative to V of 0.1 phase. b) Amplitude of variation vs. wavelength, for the three stars in

Table 3. The symbols are the same as those in Figure 4a.

Fig. 5.— a) Top left: $\Delta\text{mag}(1.25 \mu\text{m})$ vs. $\Delta\text{mag}(V)$ for the stars with at least 10 continuous weeks of optical and infrared data available. The uncertainties in V were calculated assuming ~ 0.5 magnitudes uncertainties in the AAVSO data. Note that the plotted magnitude changes do not always represent the full amplitude of the star; they are merely the observed change in magnitude over the available continuous data. b) Top right: $\Delta\text{mag}(4.9 \mu\text{m})$ vs. $\Delta\text{mag}(V)$ for the stars with at least 10 continuous weeks of optical and infrared data available. c) Second row, left: $\Delta\text{mag}(1.25 \mu\text{m})$ vs. $\Delta\text{mag}(2.2 \mu\text{m})$ for the stars with at least 10 weeks of high S/N data at both wavelengths. The magnitude changes were measured between the observed maxima and minima of the light curves, ignoring time periods during which no data were available. Note that the plotted magnitude changes do not always represent the full amplitude of the star; they are merely the observed change in magnitude over the available DIRBE data (ignoring gaps in the light curves). d) Second row, right: $\Delta\text{mag}(2.2 \mu\text{m})$ vs. $\Delta\text{mag}(3.5 \mu\text{m})$ for the stars with at least 10 weeks of high S/N data at both wavelengths. e) Third row, left: $\Delta\text{mag}(3.5 \mu\text{m})$ vs. $\Delta\text{mag}(4.9 \mu\text{m})$ for the stars with at least 10 weeks of high S/N data at both wavelengths. f) Third row, right: $\Delta\text{mag}(4.9 \mu\text{m})$ vs. $\Delta\text{mag}(12 \mu\text{m})$ for the stars with at least 10 weeks of high S/N data at both wavelengths. g) Fourth row, left: $\Delta\text{mag}(12 \mu\text{m})$ vs. $\Delta\text{mag}(25 \mu\text{m})$ for the stars with at least 10 weeks of high S/N data at both wavelengths.

TABLE 1
 CARBON-RICH MIRA VARIABLE STARS IN SAMPLE

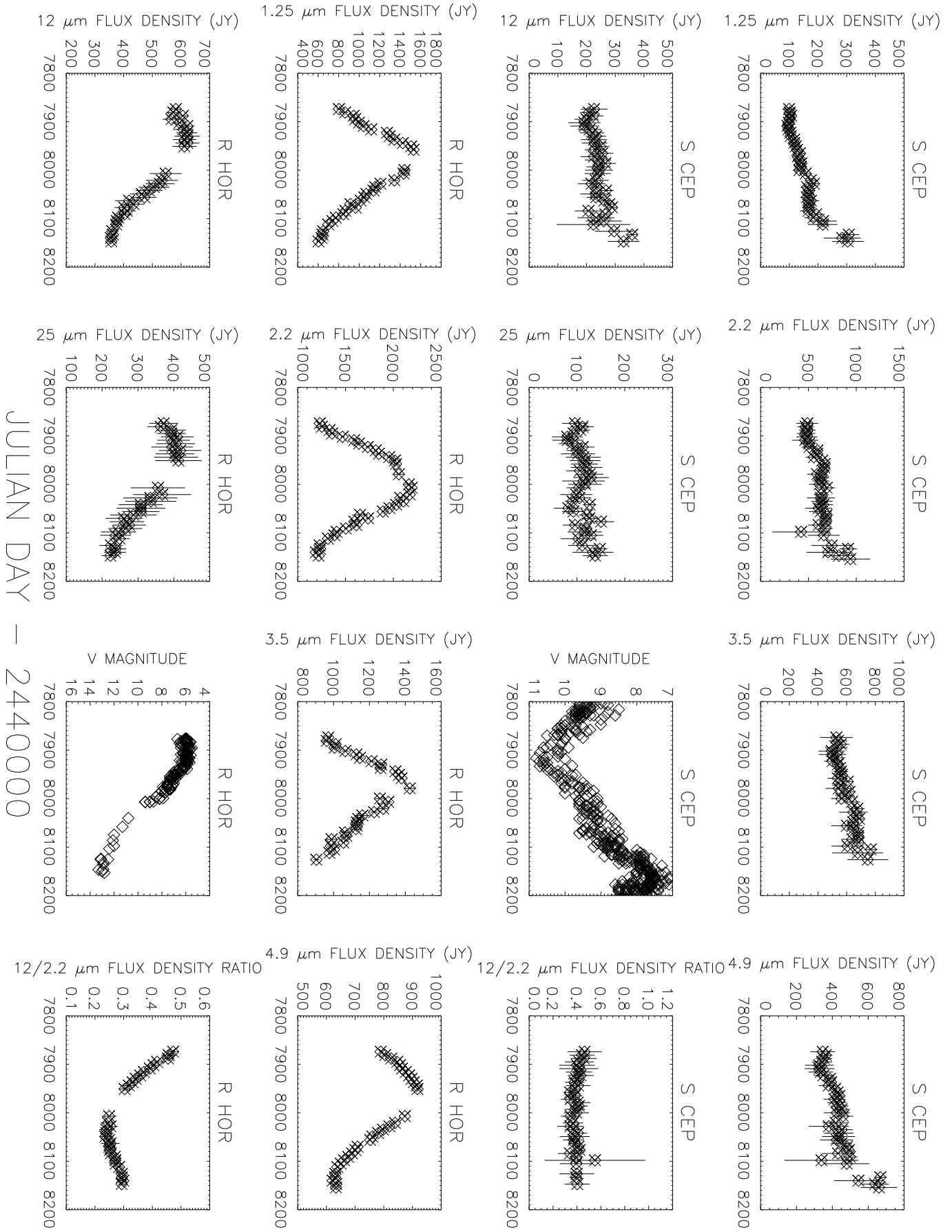
Name	Period (Days)	[12] (mag)	Spectral Type	Dust Spectrum	Optical Data?
R For	388.73	-2.38	C4,3e(Ne)	SiC	Yes
V384 Per	535.0	-3.19	C(N)	SiC	
R Lep	427.07	-2.82	C7,6e(N6e)	SiC	Yes
V Cyg	421.27	-3.43	C5,3e-C7,4e(Npe)	SiC	Yes
RV Aqr	453.50	-2.59	C6-7,2-4(Ne)	SiC	
V1426 Cyg	470.0	-2.40	C7,2e(N)	SiC	
S Cep	486.84	-2.83	C7.4e,(N8e)	SiC+:	Yes
LP And		-3.83	C8,3.5e	Red	

TABLE 2
OXYGEN-RICH MIRA VARIABLE STARS IN SAMPLE

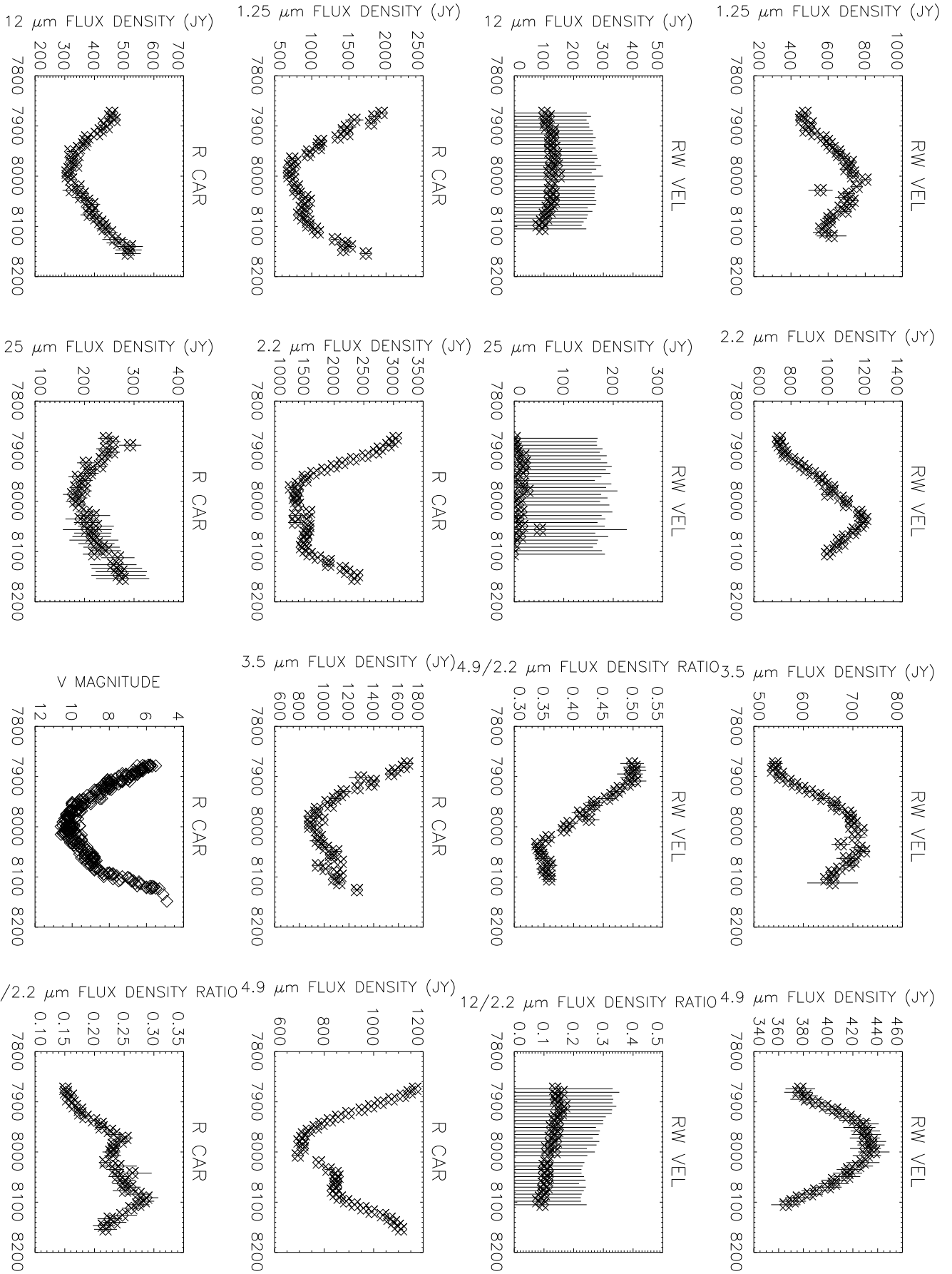
Name	Period (Days)	[12] (mag)	Spectral Type	Dust Spectrum	Optical Data?
KU And	750.00	-3.06	M10 I-III	SE5	
T Cas	444.83	-2.95	M6-9.0e	SE1	Yes
WX Psc	660.00	-4.03	M8	SB	
o Cet	331.96	-5.59	M5-9e	SE8	Yes
R Hor	407.60	-3.53	M5-8eII-III	SE5t	Yes
IK Tau	470.00	-5.54	M6-10e	SE7	Yes
TX Cam	557.40	-4.41	M8-10	SE6	Yes
R Aur	457.51	-3.03	M6.5-9.5e	SE2	Yes
U Ori	368.30	-3.46	M6-9.5e	SE6t	Yes
GX Mon	527.00	-3.32	M9	SE6	
R Cnc	361.60	-2.54	M6-9e	SE2	Yes
RW Vel	443.10	-2.34	M7 III(II)e	SE2	
R Car	308.71	-3.06	M4-8e	SE1	Yes
R LMi	372.19	-2.94	M6.5-9.0e(Tc:)	SE4t	Yes
IW Hya	650.00	-3.32	M9	SE5	
R Leo	309.95	-4.71	M6-8 III-9.5e	SE2	Yes
AQ Cen	387.50	-2.32	Me	SE7	
R Cen	546.20	-3.09	M4-8IIe	SE2	Yes
WX Ser	425.10	-2.30	M8e	SE6	
U Her	406.10	-3.12	M6.5-9.5e	SE4	Yes
V1111 Oph		-3.51	M4III-9	SE5	
X Oph	328.85	-2.90	M5-9e	SE1	Yes
V3953 Sgr		-3.39	M9	SE6	
R Aql	284.20	-2.88	M5-9e	SE5	Yes
V3880 Sgr	510.00	-2.53	M8:	SE5	
V342 Sgr	372.00	-2.63	M9	SE6	
RR Aql	394.78	-2.67	M6e-9	SE7	Yes
T Cep	388.14	-3.56	M5.5-8.8e	SE1	Yes
R Aqr	386.96	-4.37	M5-8.5e+peC	SE7	Yes
R Cas	430.46	-4.19	M6-10e	SE5t	Yes

TABLE 3
PARAMETERS OF BEST-FIT SINE CURVES

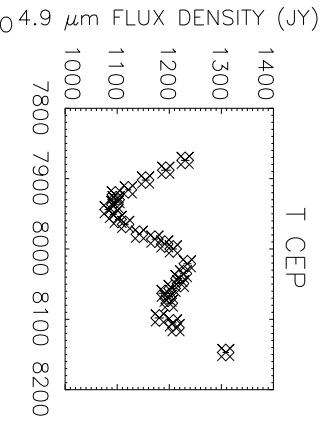
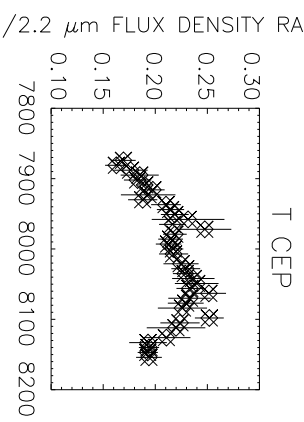
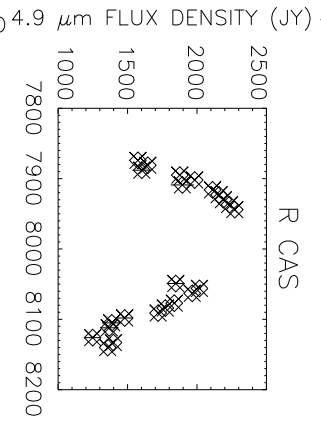
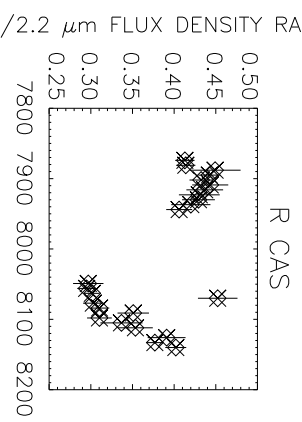
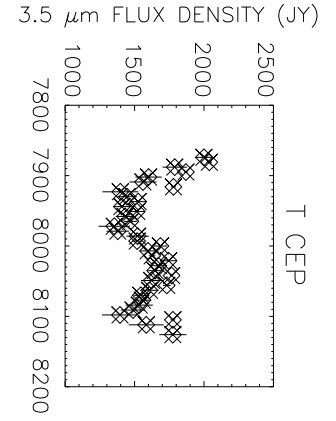
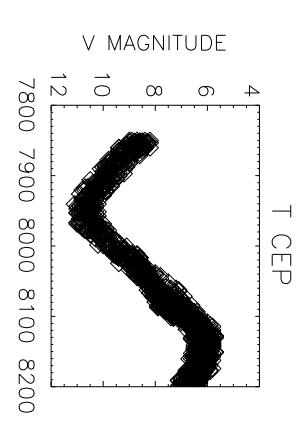
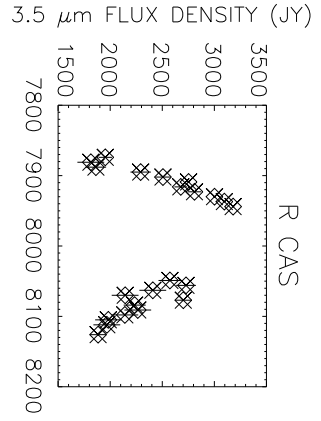
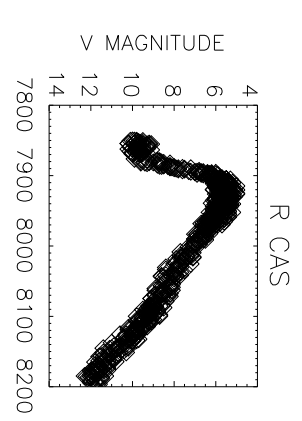
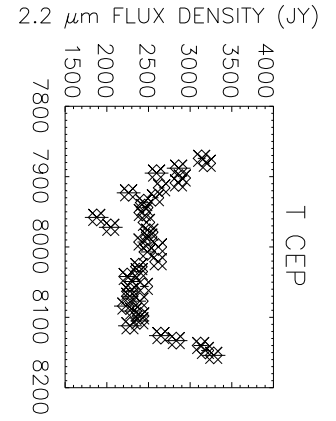
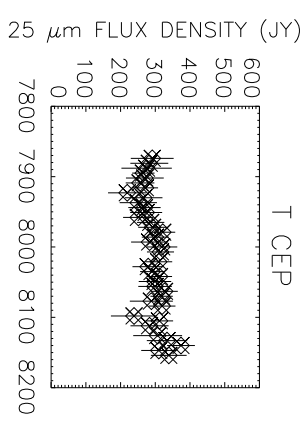
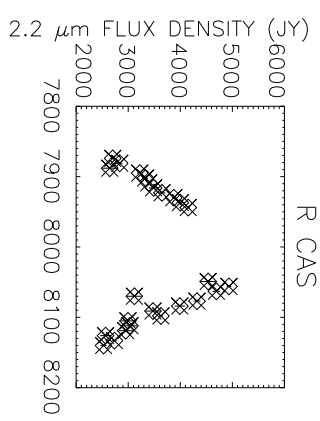
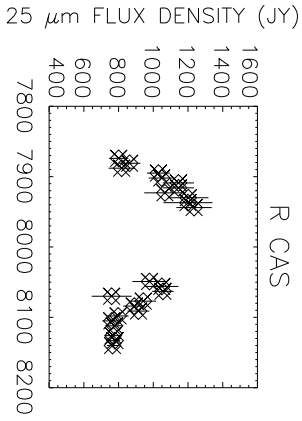
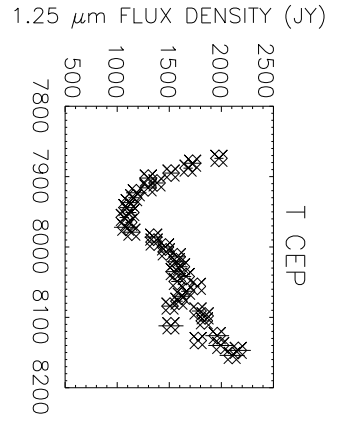
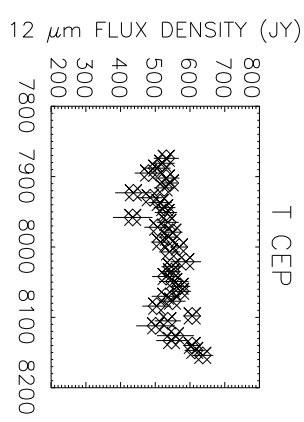
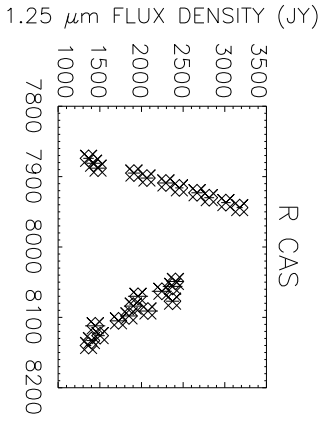
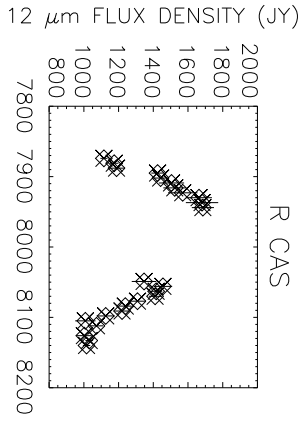
Star	Wavelength (μm)	Date of Maximum (JD)	Amplitude (Magnitudes)
R Hor	0.55	2447934	7.66
	1.25	2447987	1.14
	2.2	2447999	0.83
	3.5	2447993	0.56
	4.9	2447959	0.45
	12	2447939	0.59
	25	2447960	0.64
R Cas	0.55	2447957	5.53
	1.25	2447994	1.42
	2.2	2448003	1.03
	3.5	2447995	0.84
	4.9	2447982	0.77
	12	2447978	0.70
	25	2447980	0.68
RW Vel	1.25	2448013	0.80
	2.2	2448032	0.59
	3.5	2448025	0.41
	4.9	2447983	0.29

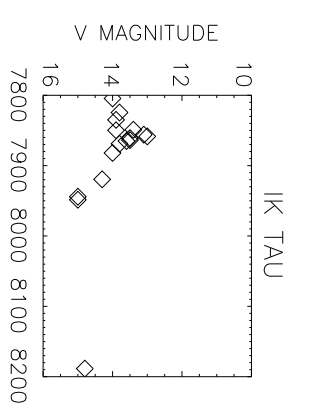
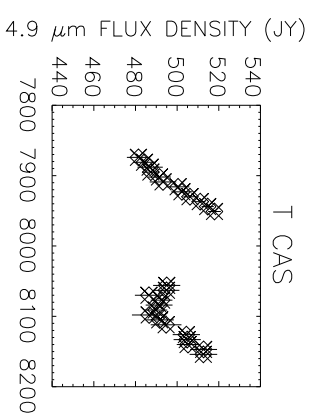
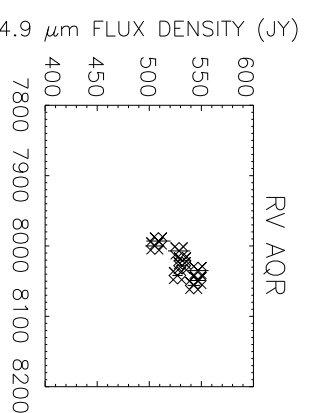
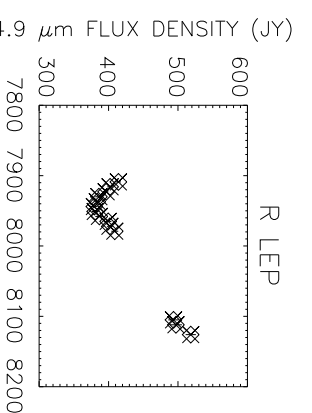
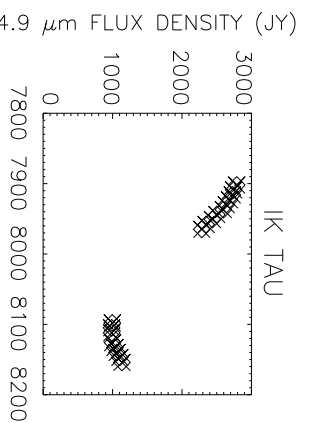
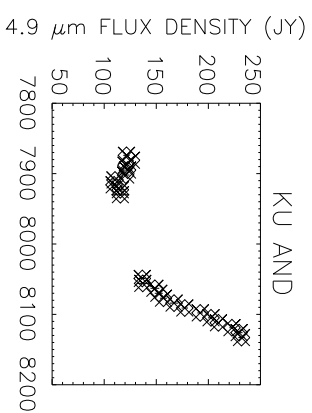
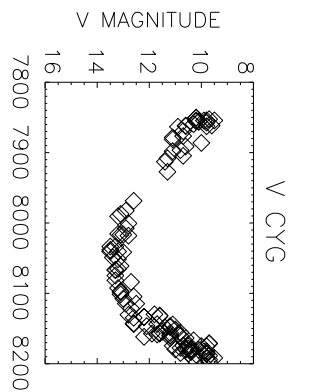
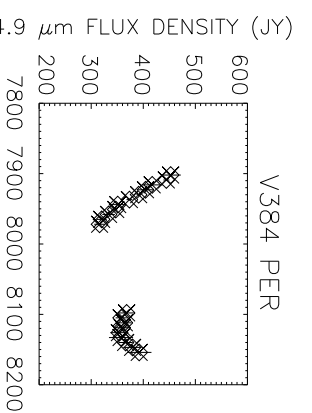
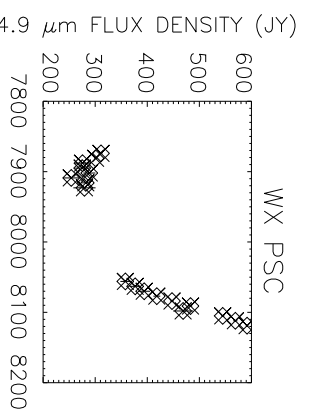
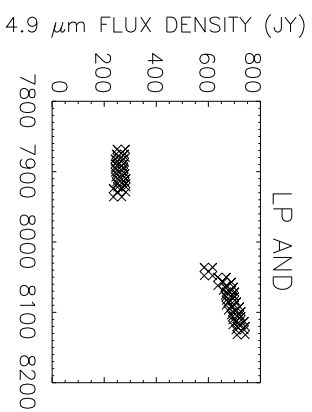
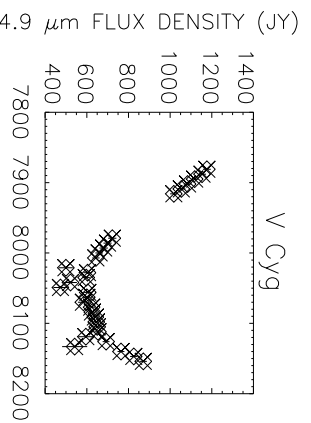
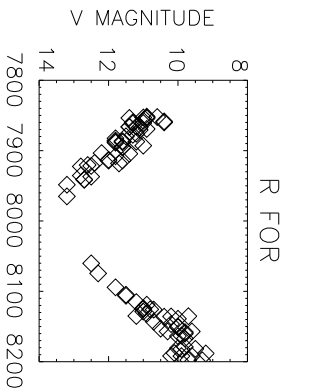
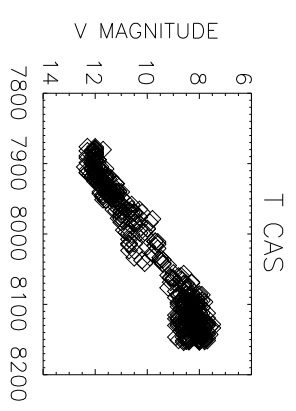
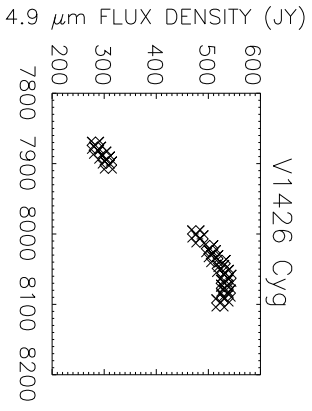
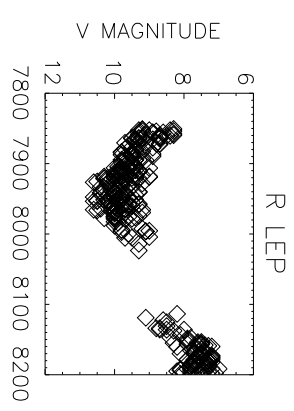
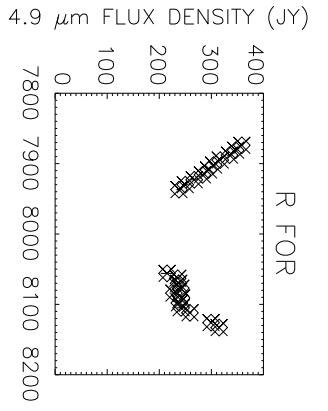


JULIAN DAY - 2440000



JULIAN DAY - 2440000

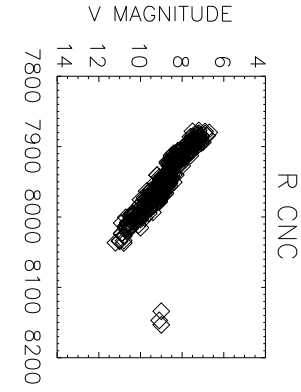
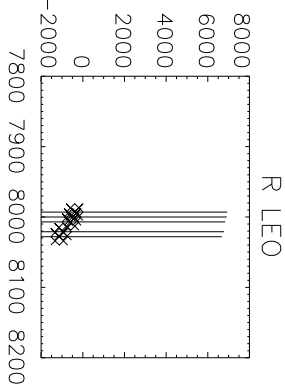




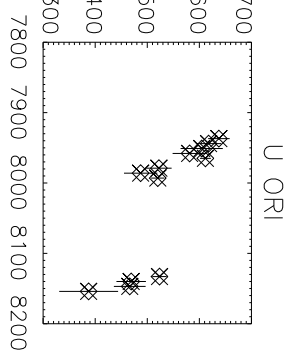
JULIAN DAY - 2440000

JULIAN DAY - 2440000

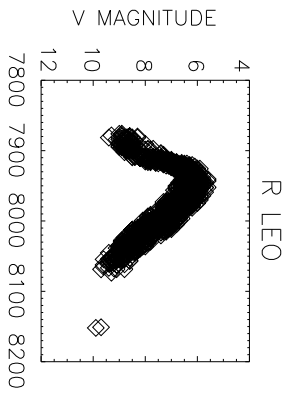
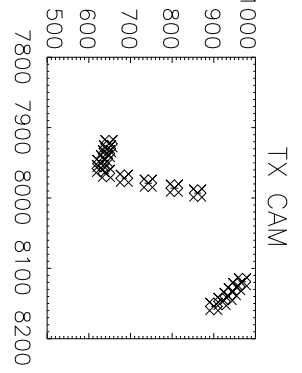
4.9 μm FLUX DENSITY (JY)



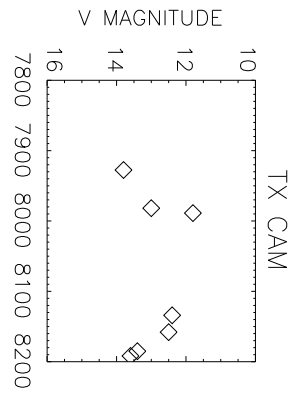
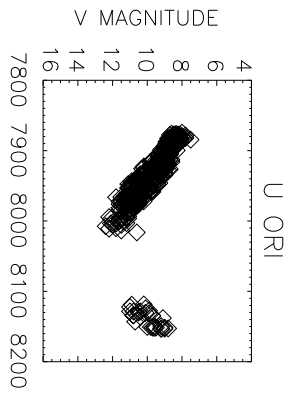
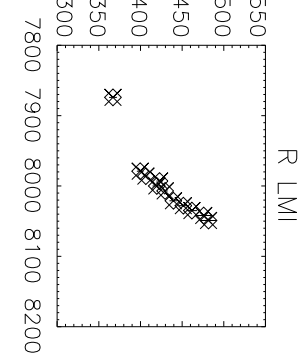
4.9 μm FLUX DENSITY (JY)



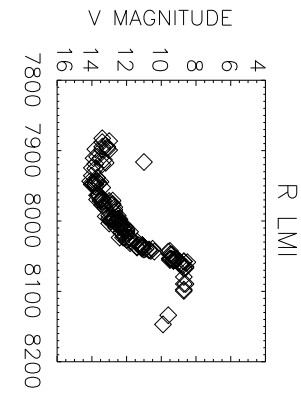
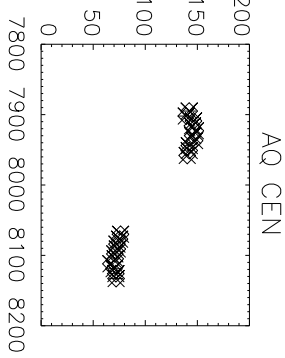
4.9 μm FLUX DENSITY (JY)



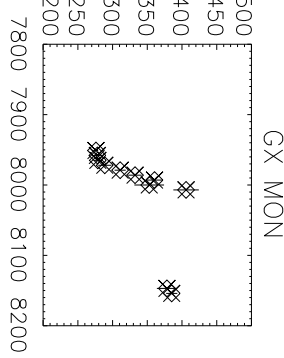
4.9 μm FLUX DENSITY (JY)



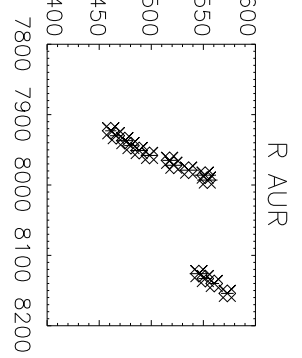
4.9 μm FLUX DENSITY (JY)



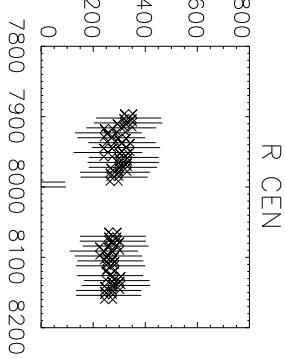
4.9 μm FLUX DENSITY (JY)



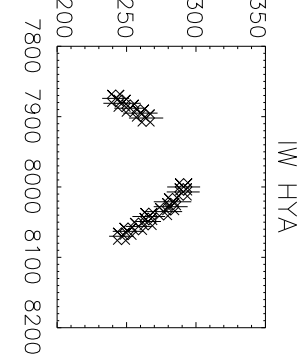
4.9 μm FLUX DENSITY (JY)



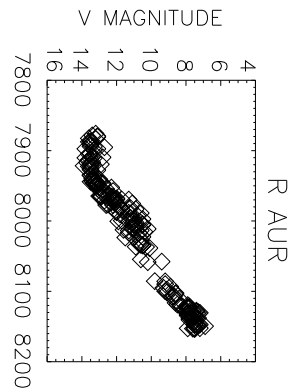
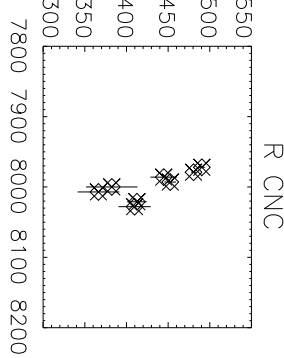
4.9 μm FLUX DENSITY (JY)



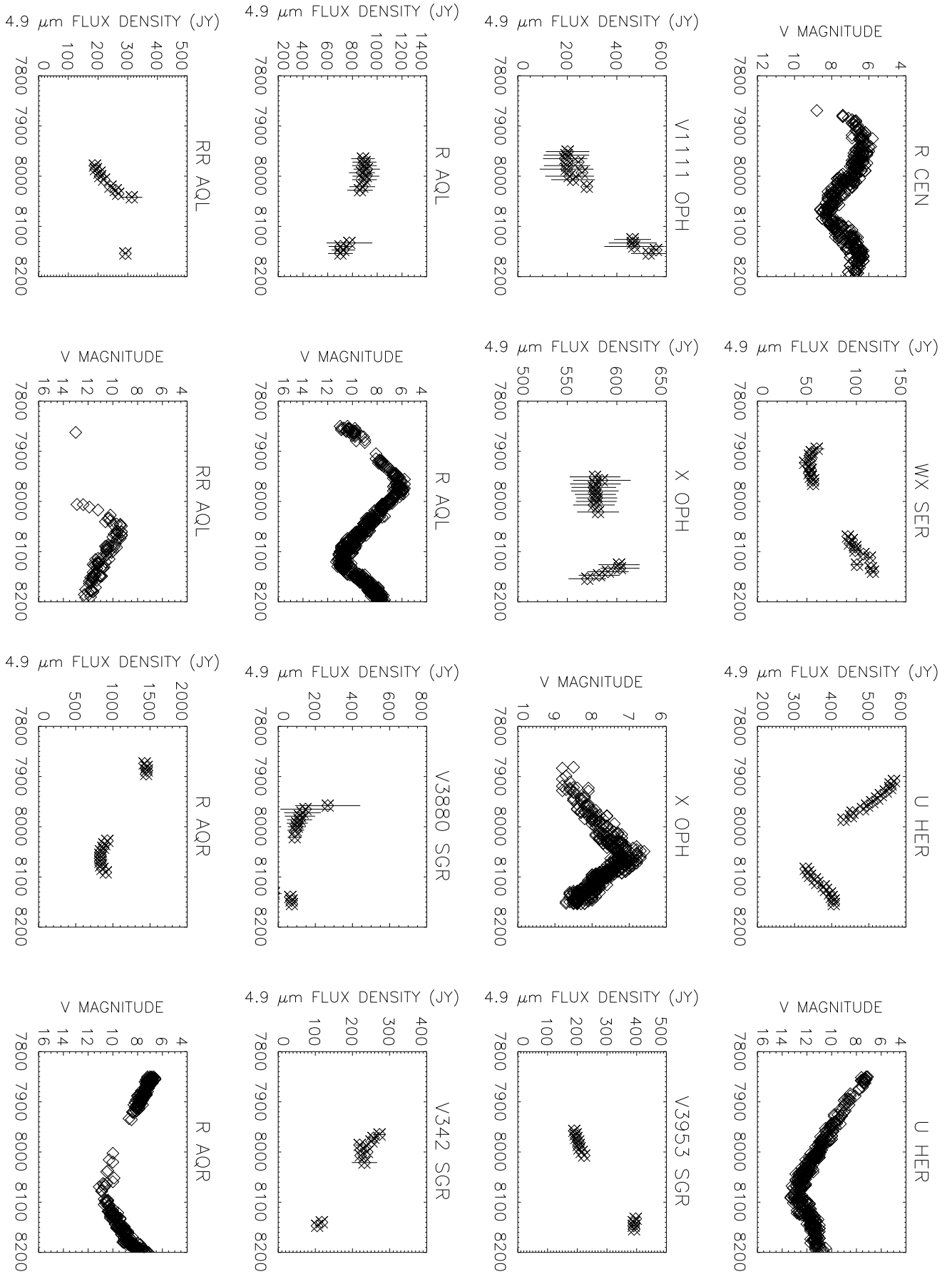
4.9 μm FLUX DENSITY (JY)



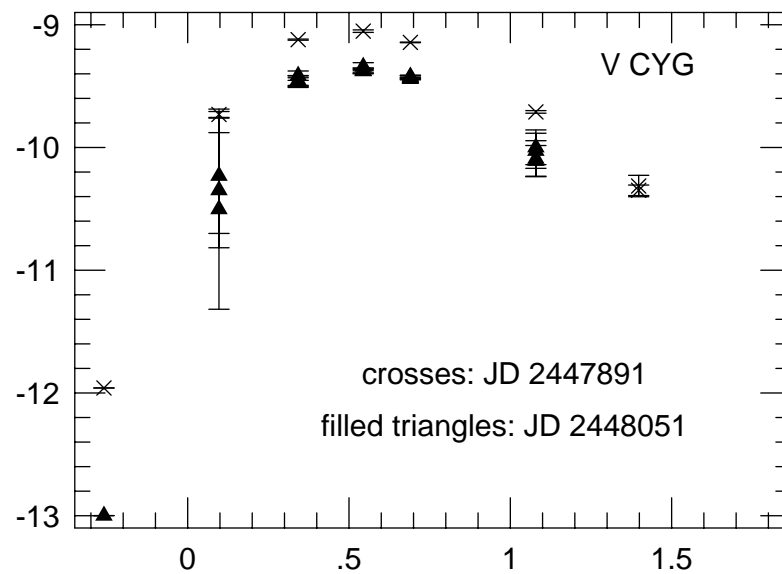
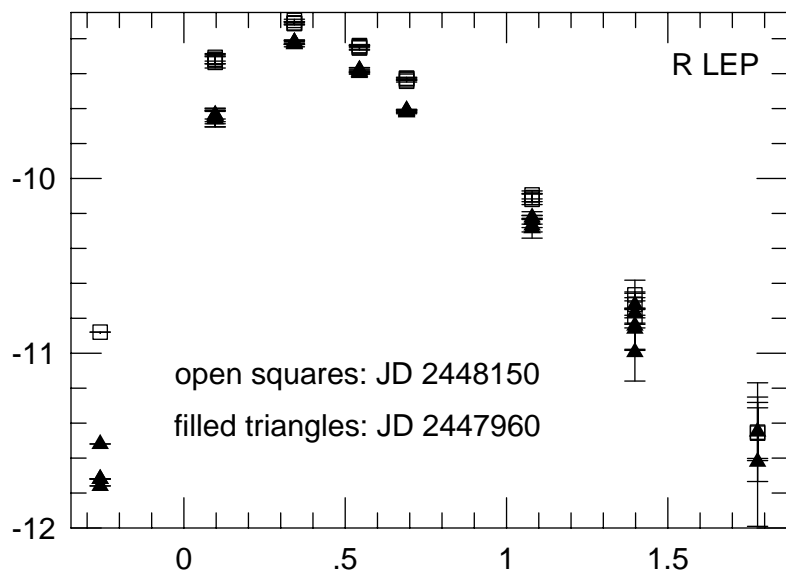
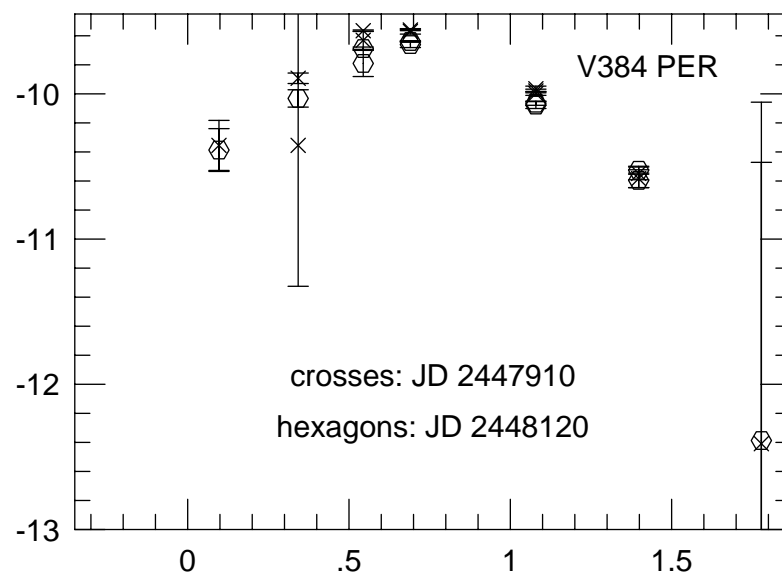
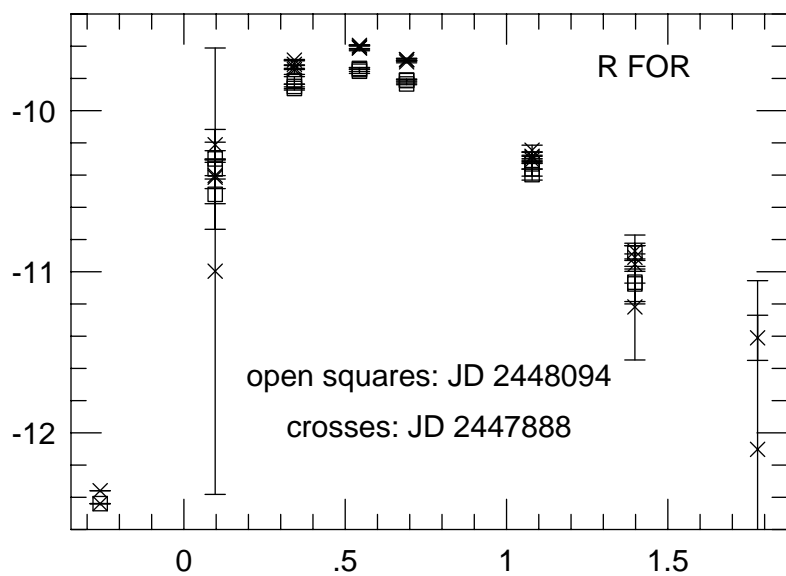
4.9 μm FLUX DENSITY (JY)



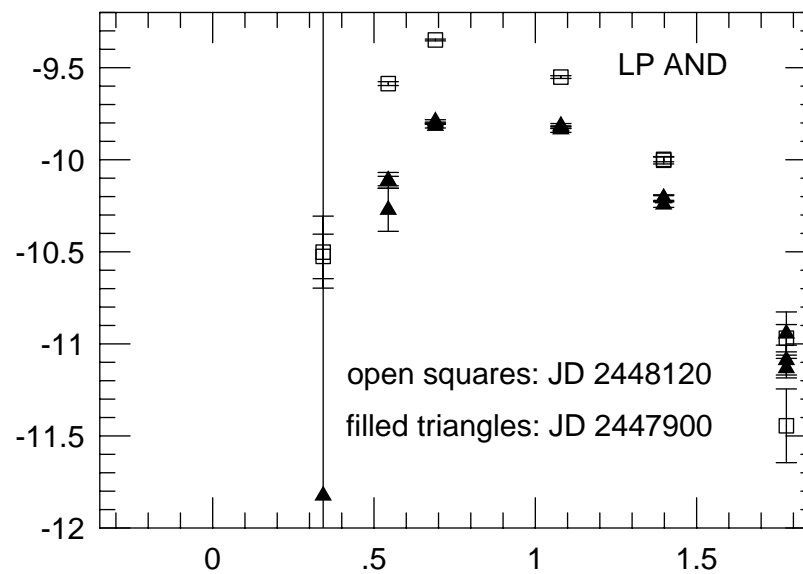
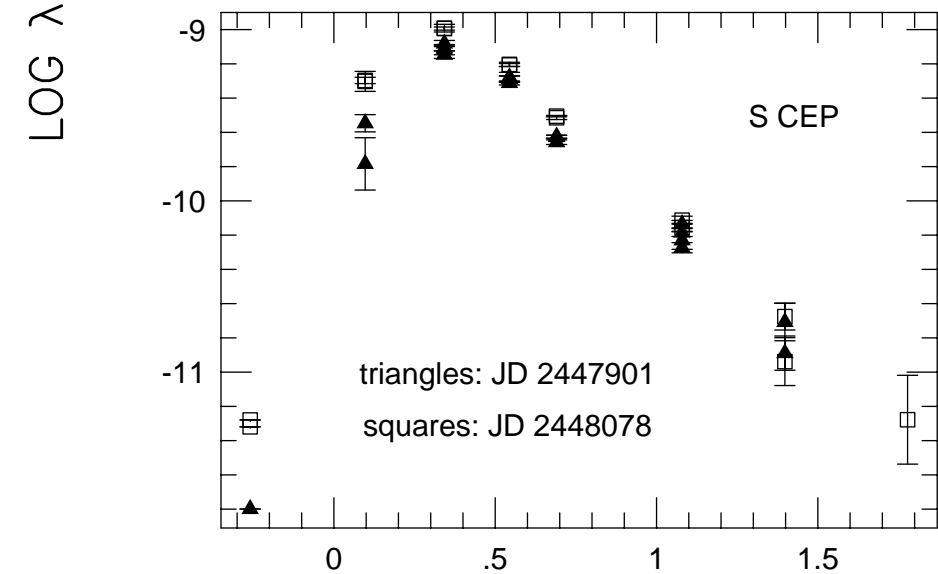
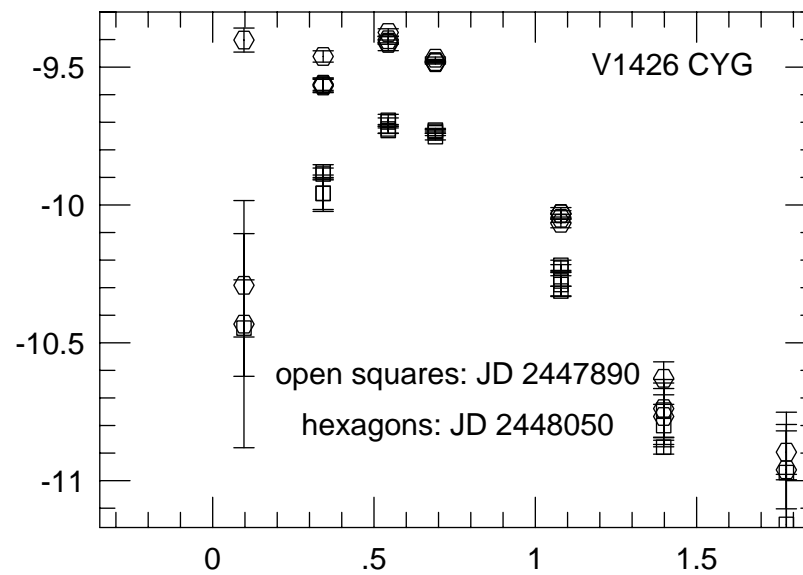
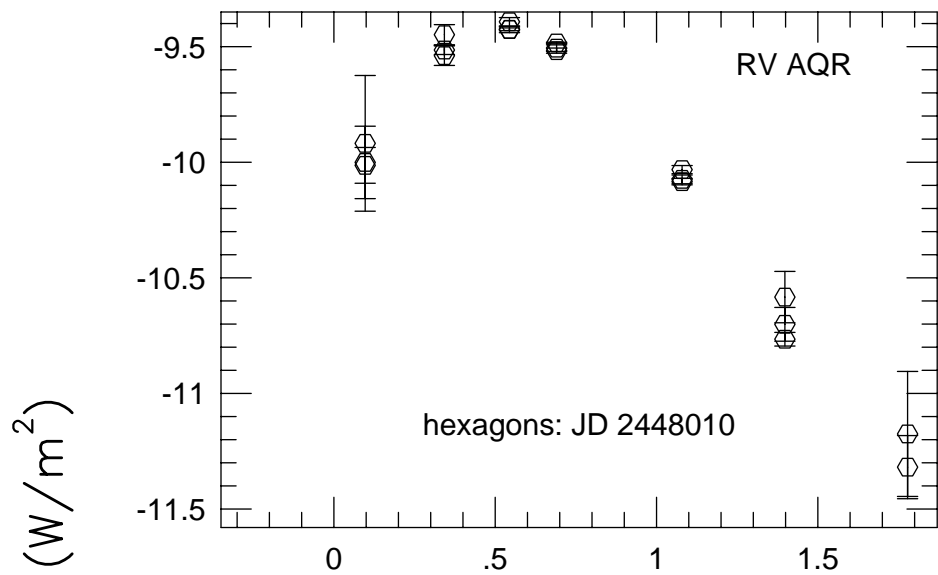
JULIAN DAY - 2440000



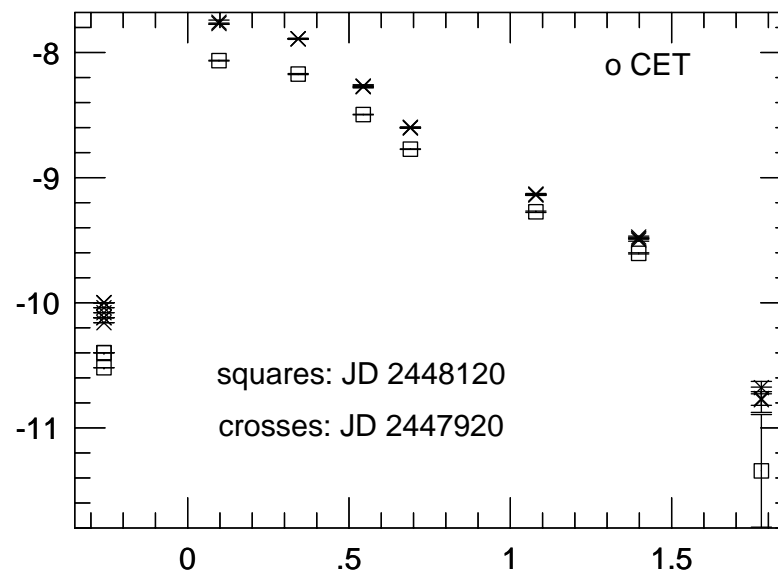
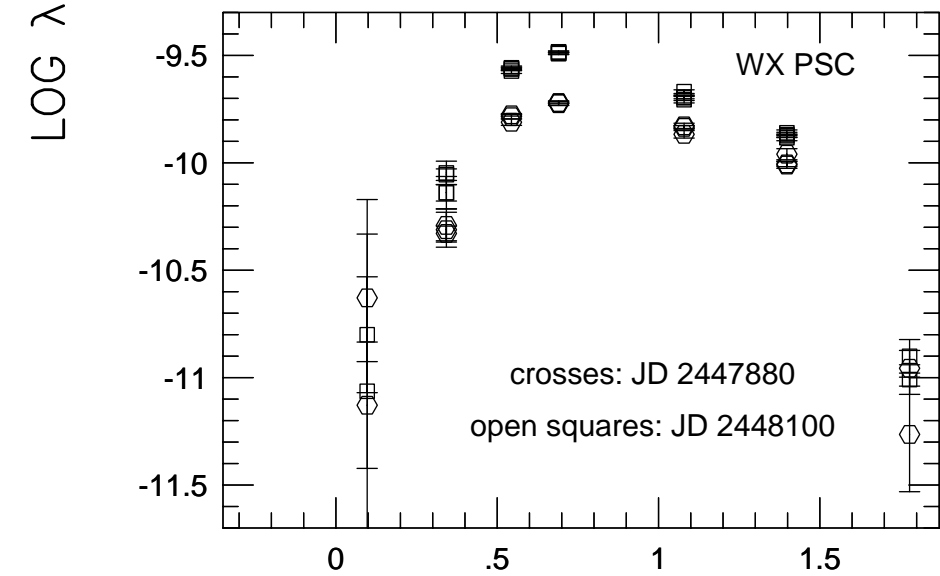
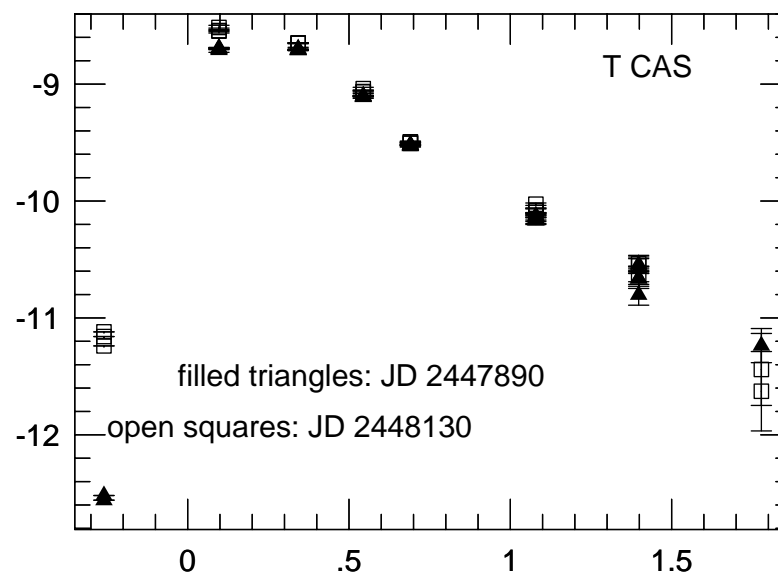
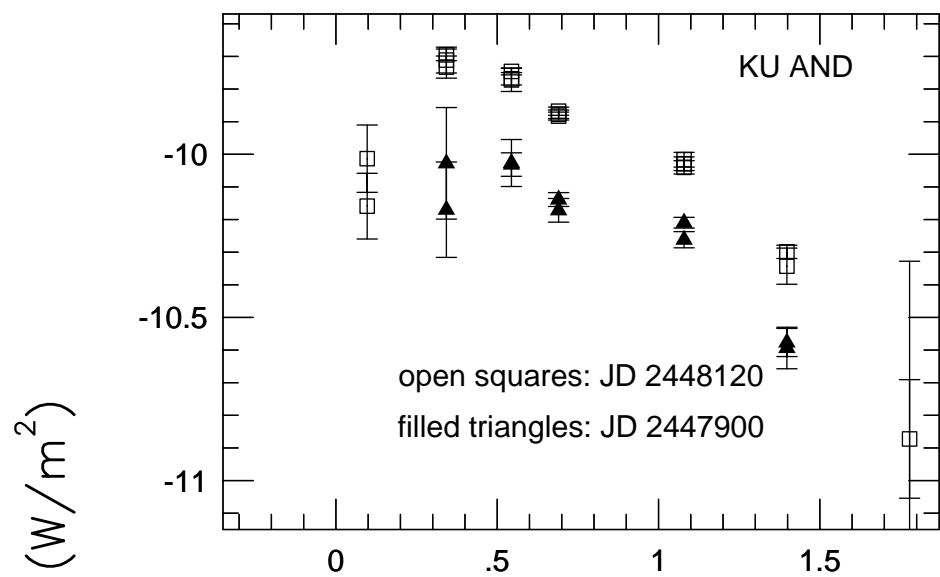
LOG λF_λ (W/m^2)



LOG WAVELENGTH (μm)

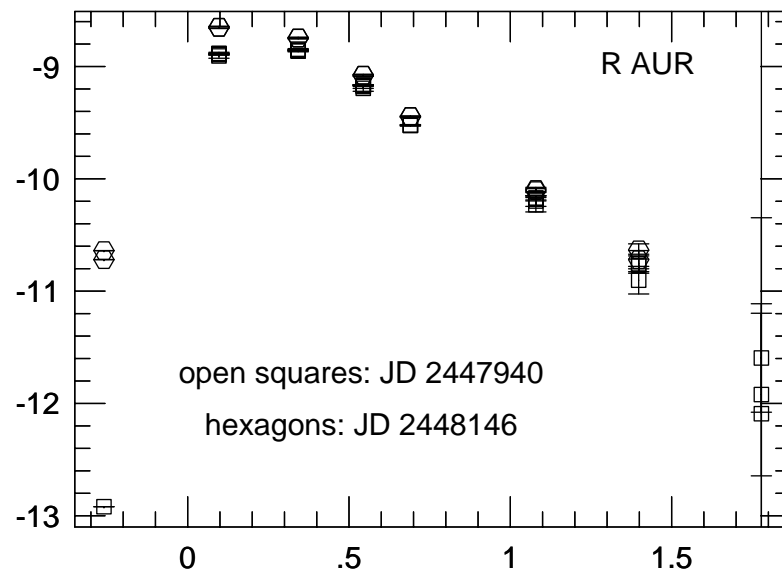
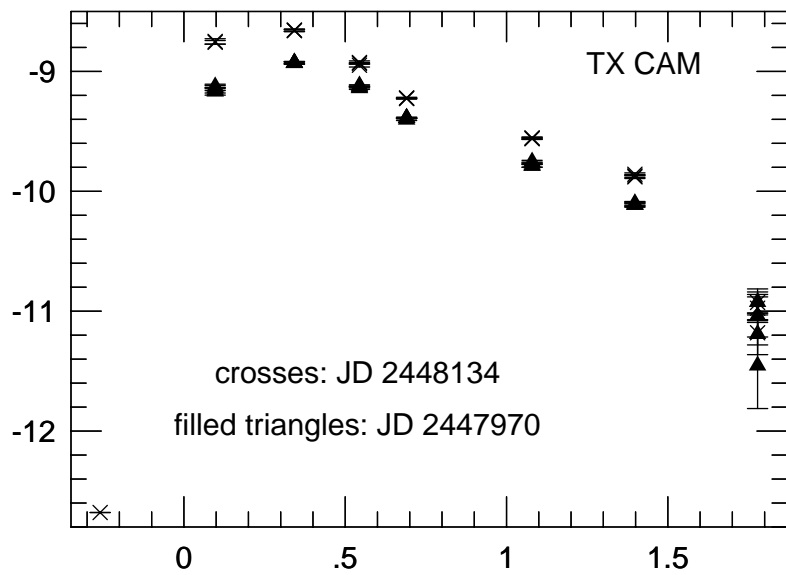
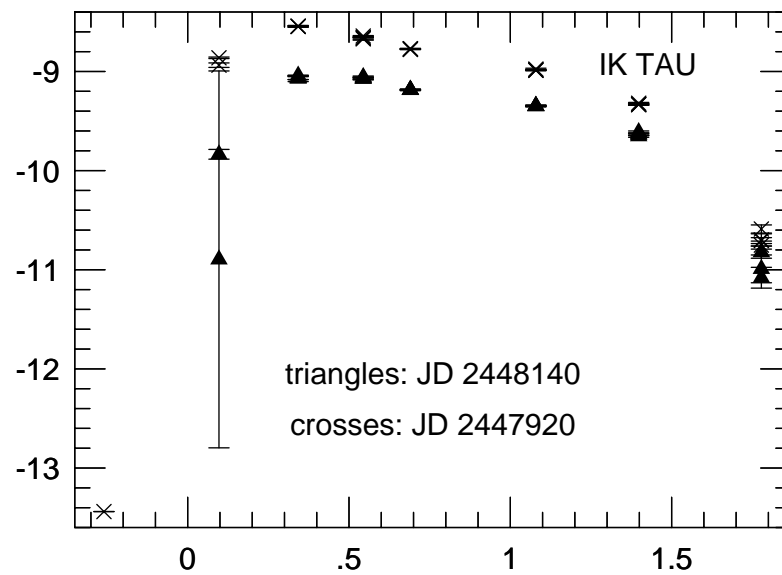
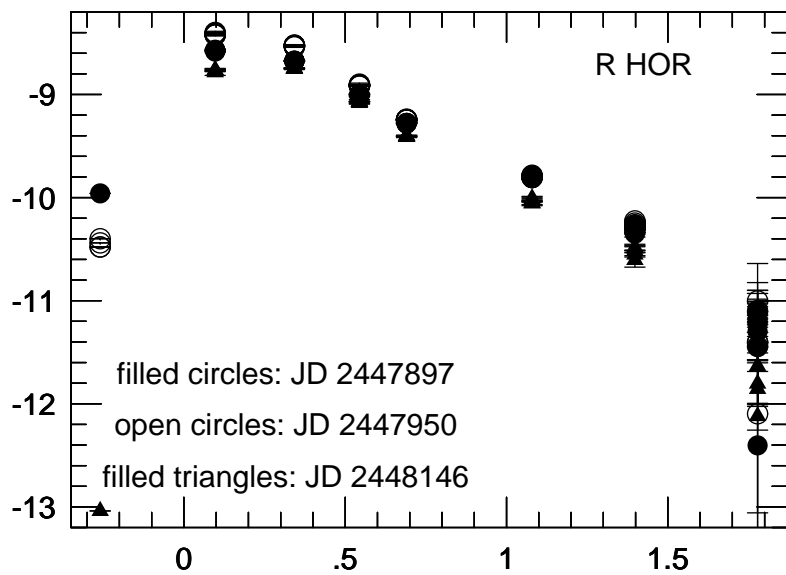


LOG WAVELENGTH (μm)

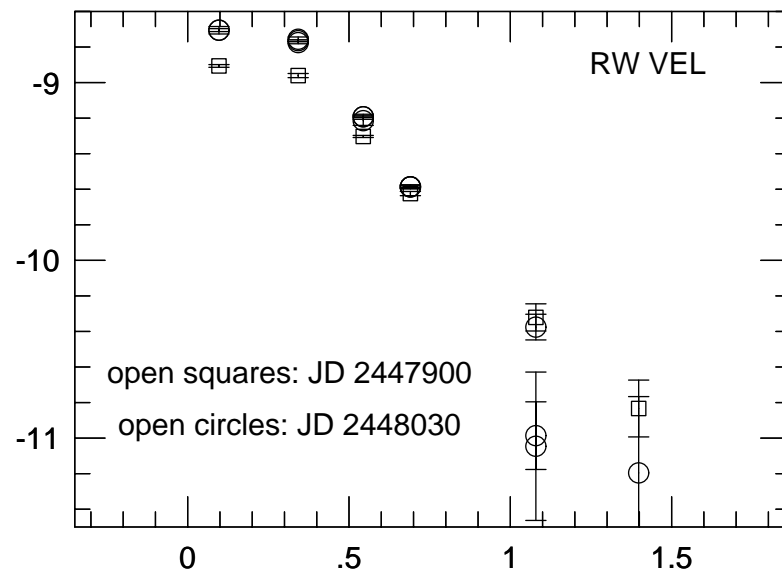
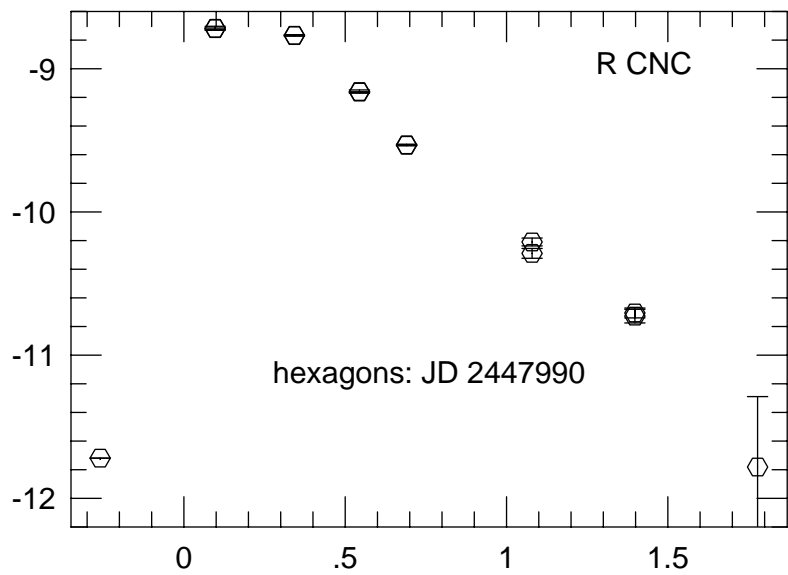
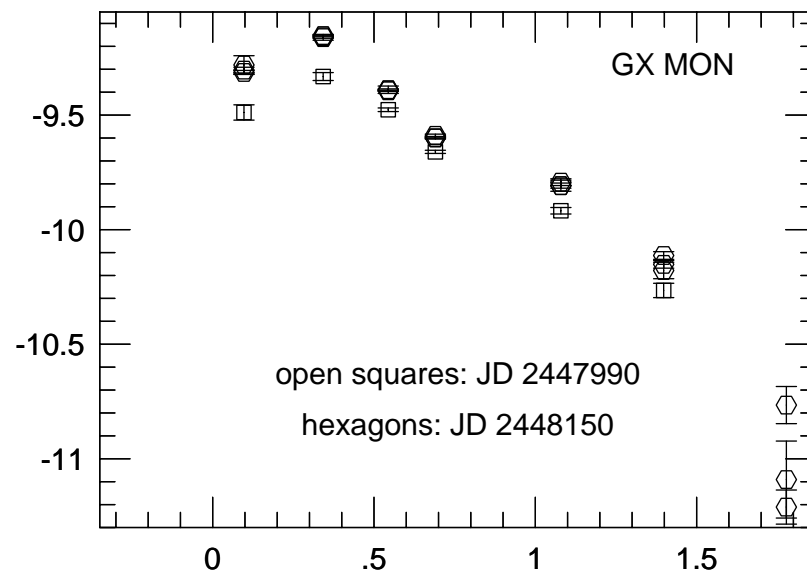
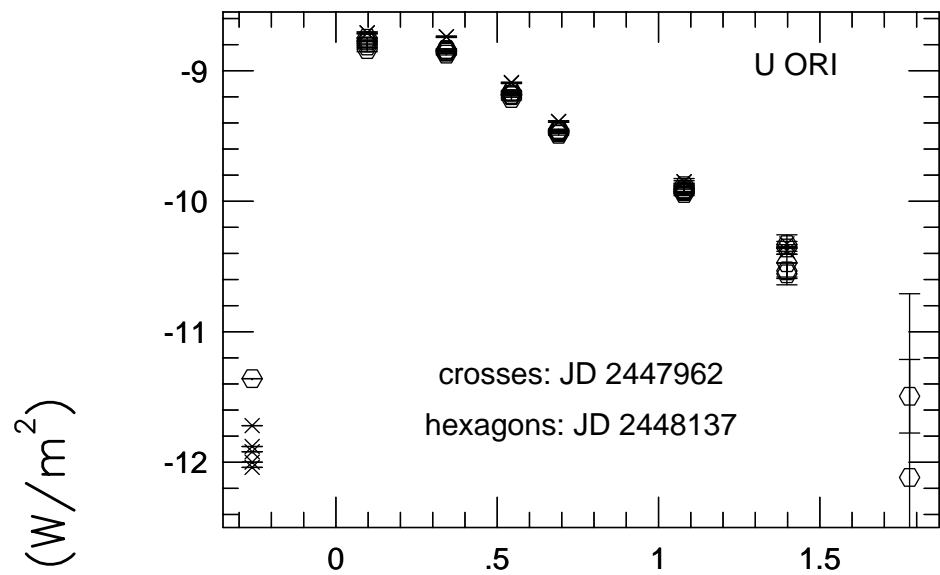


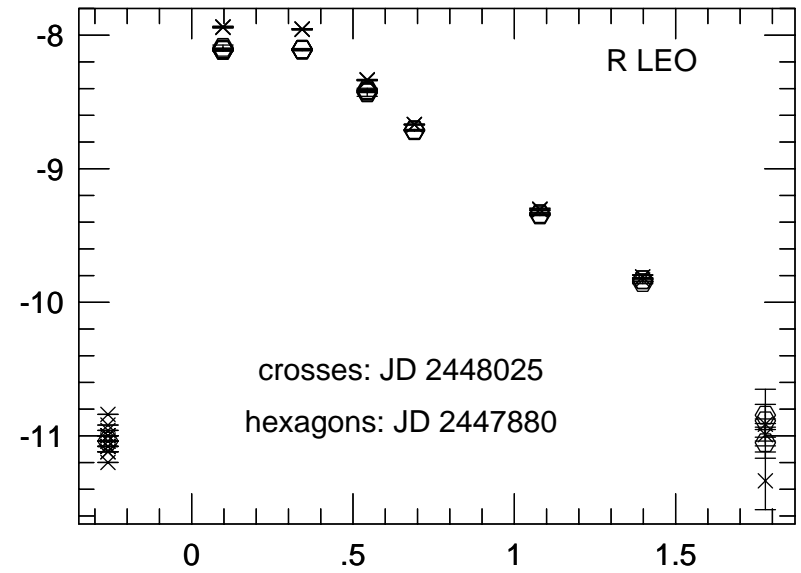
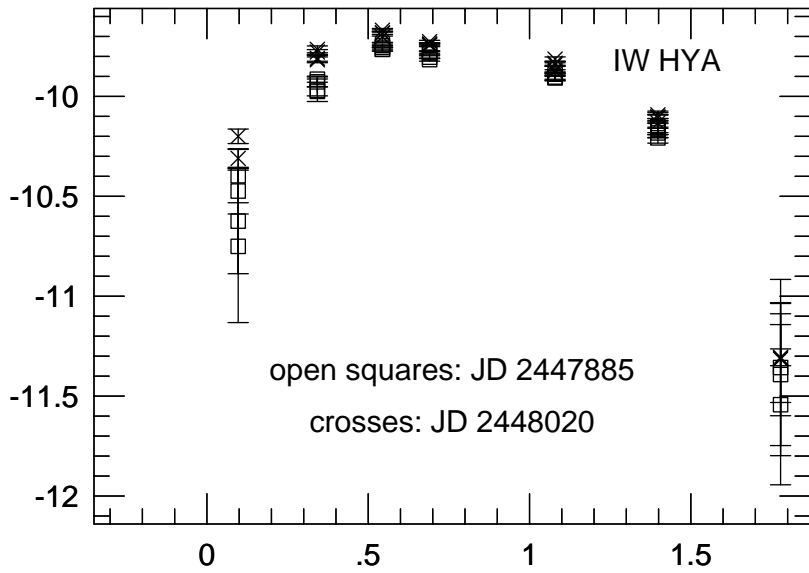
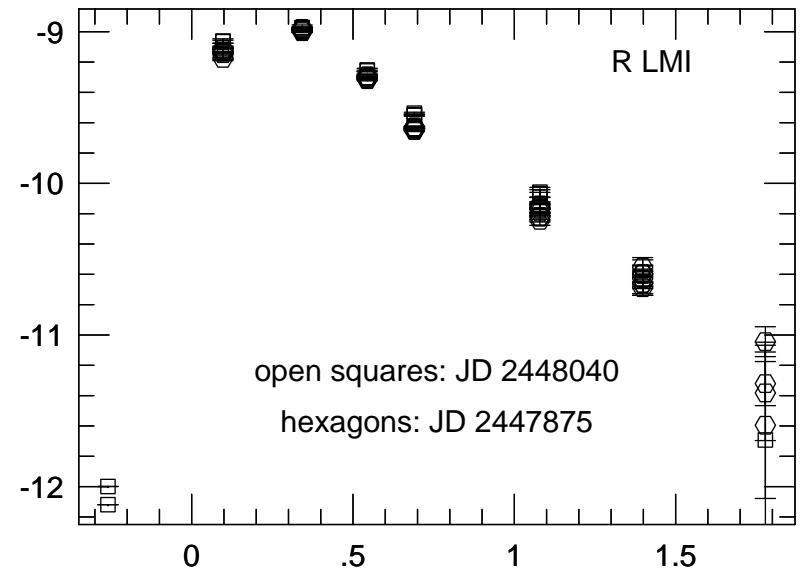
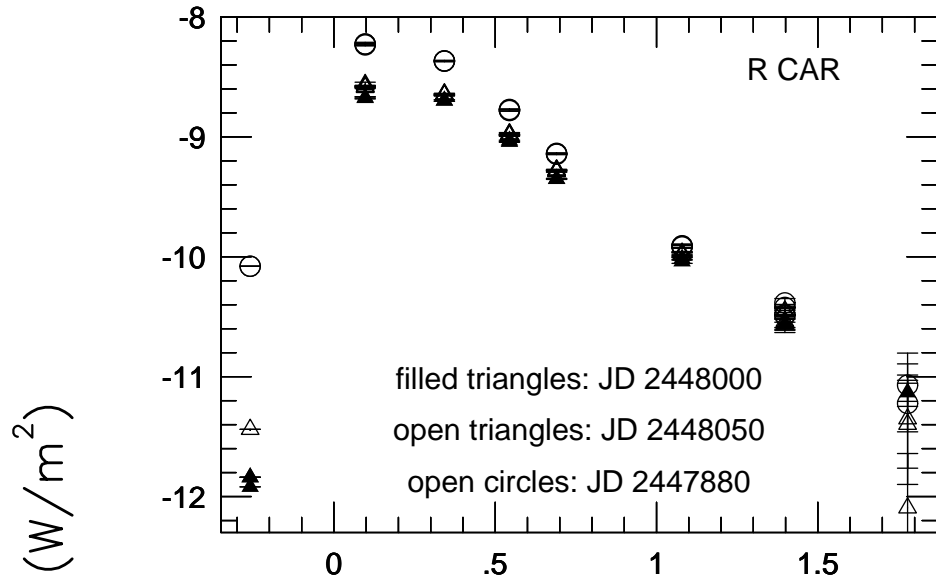
LOG WAVELENGTH (μm)

LOG λF_{λ} (W/m^2)

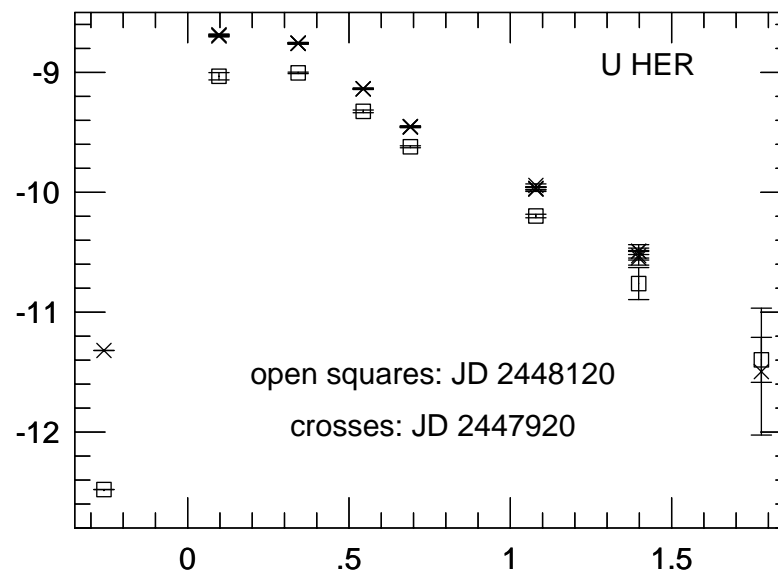
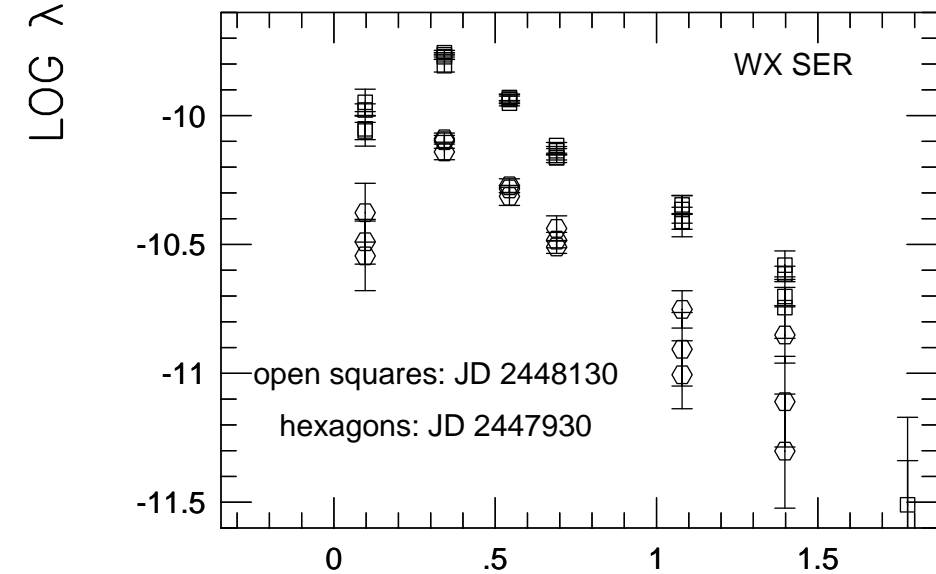
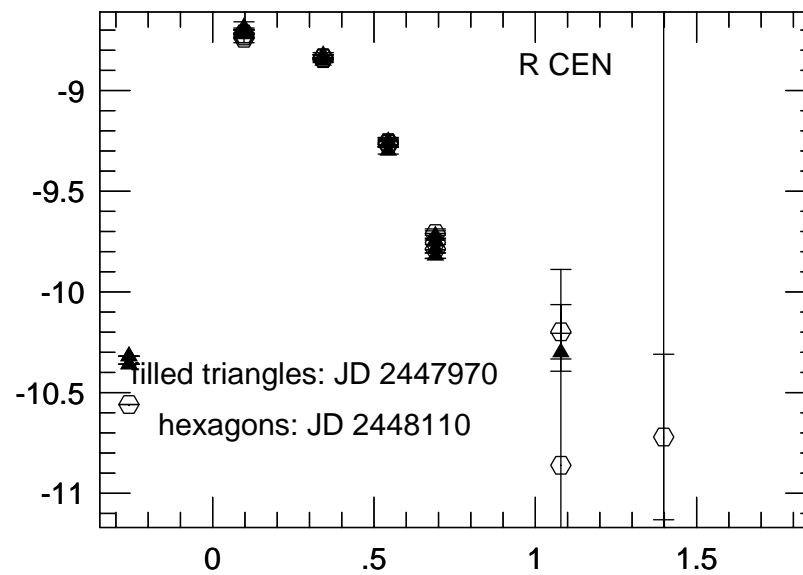
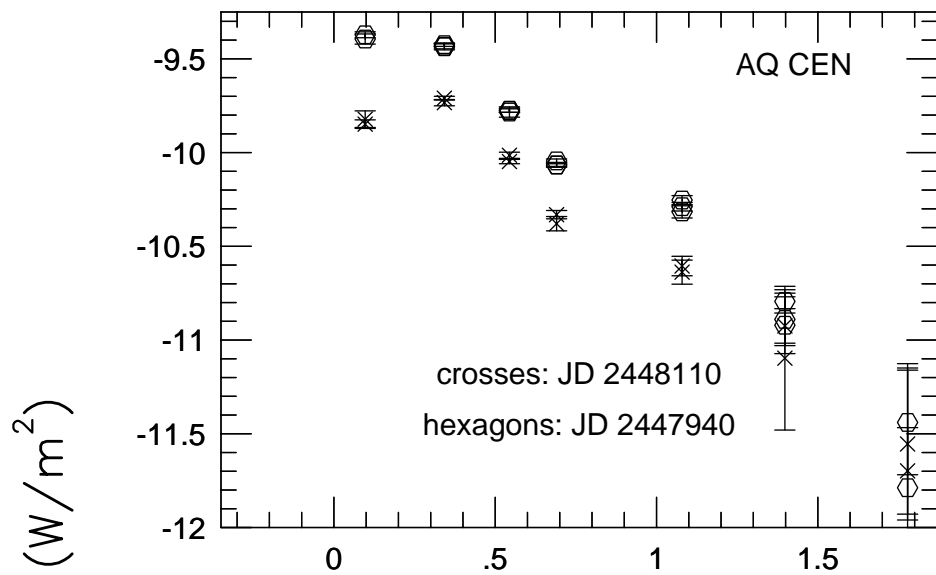


LOG WAVELENGTH (μm)

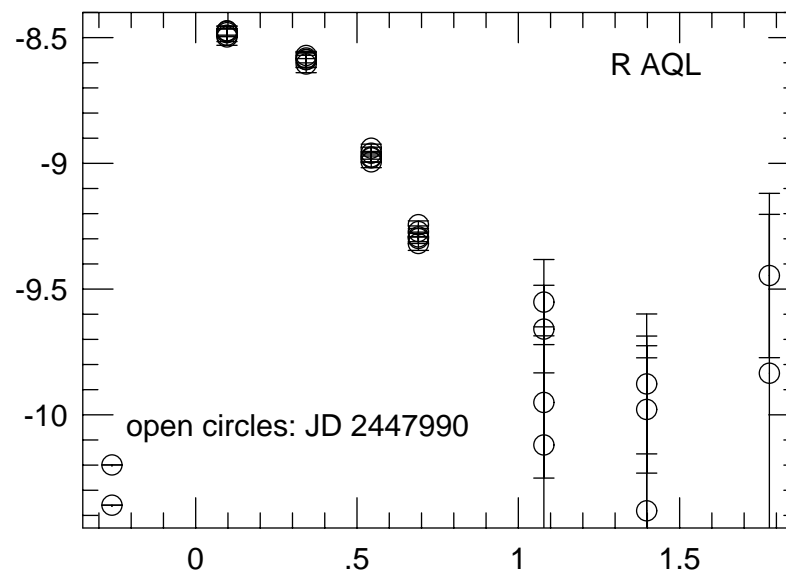
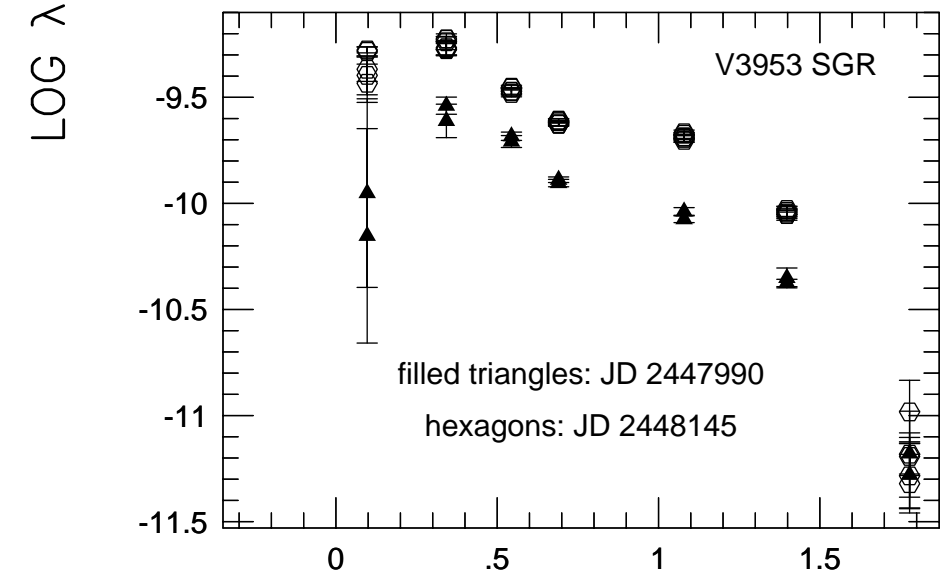
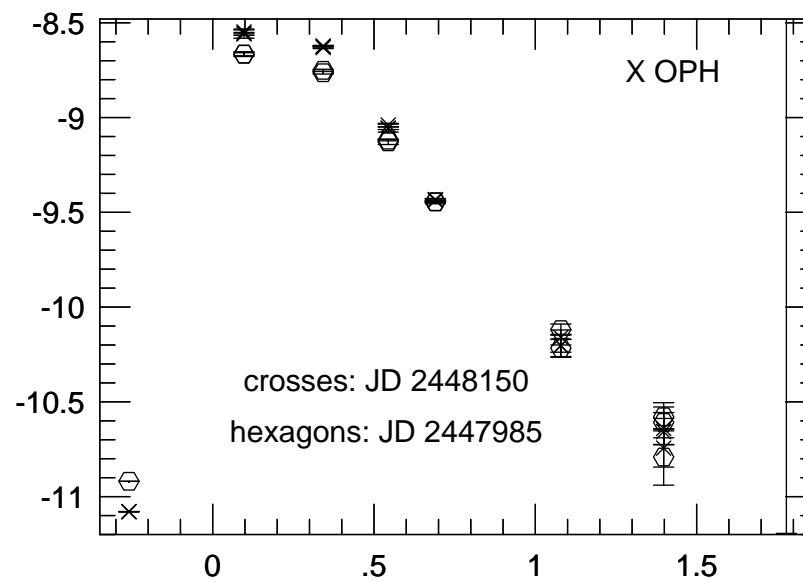
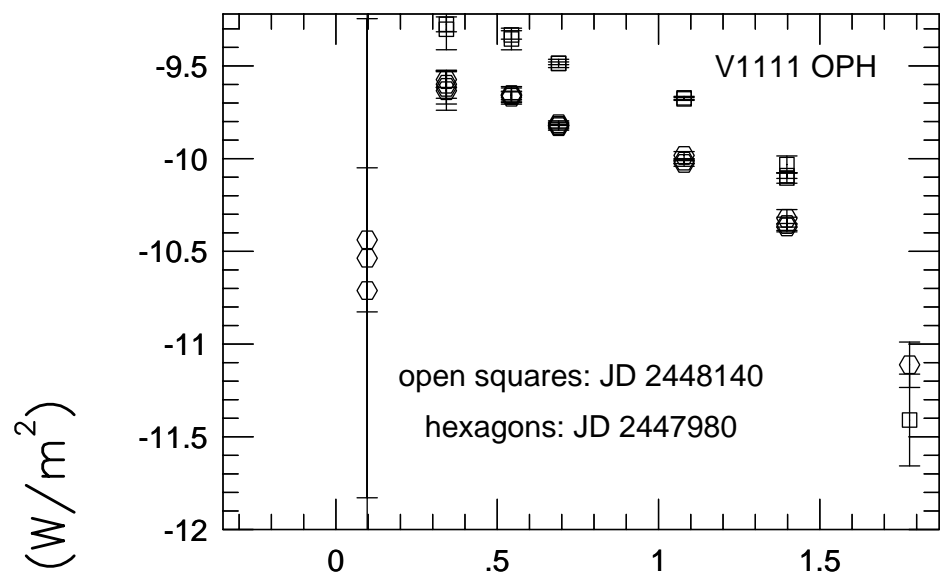




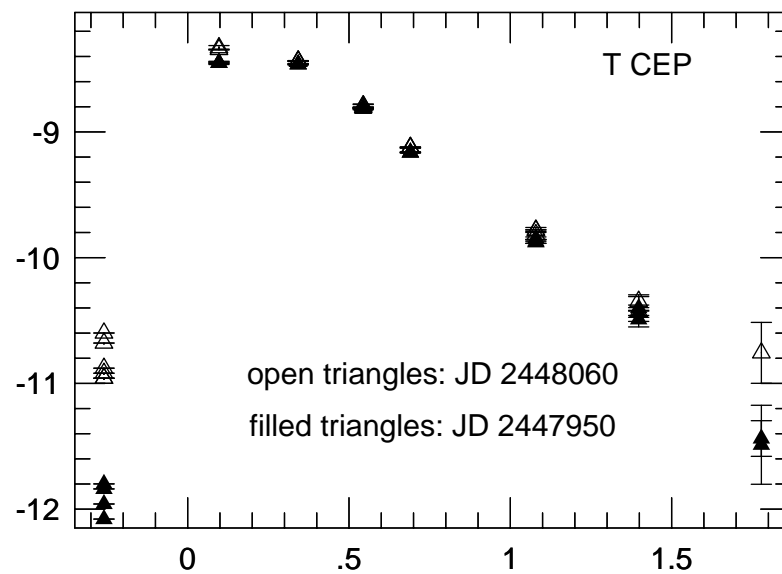
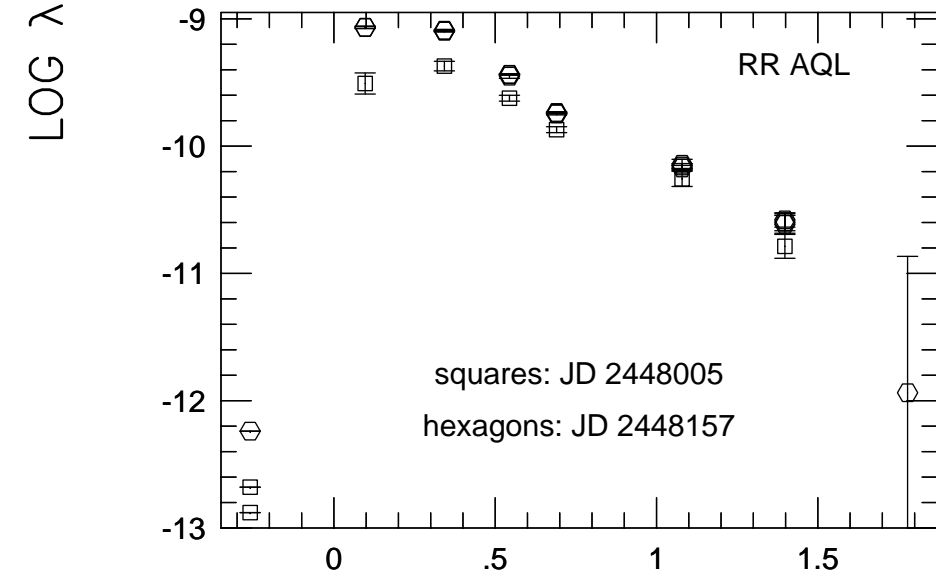
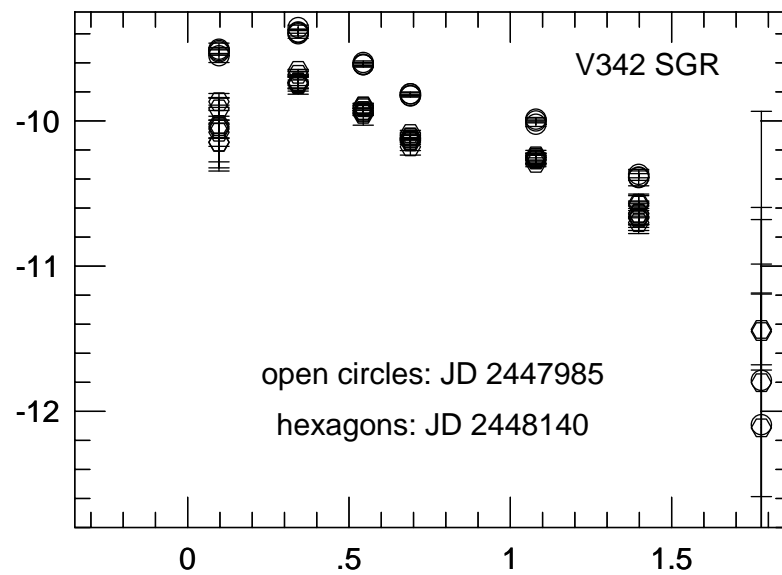
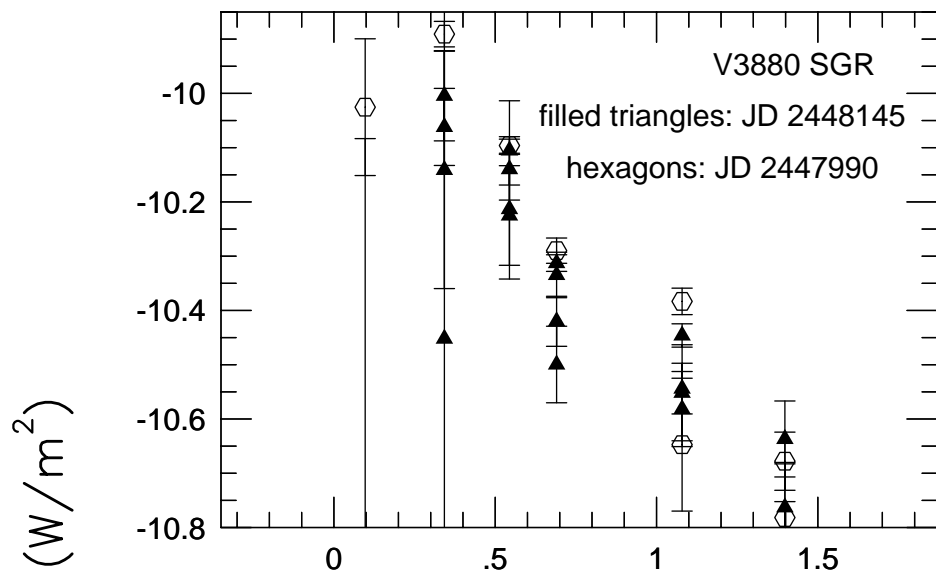
LOG WAVELENGTH (μm)



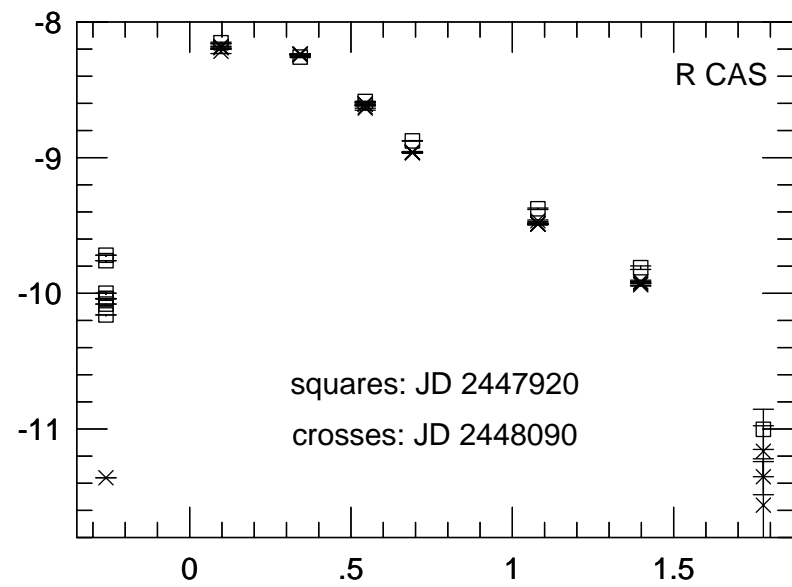
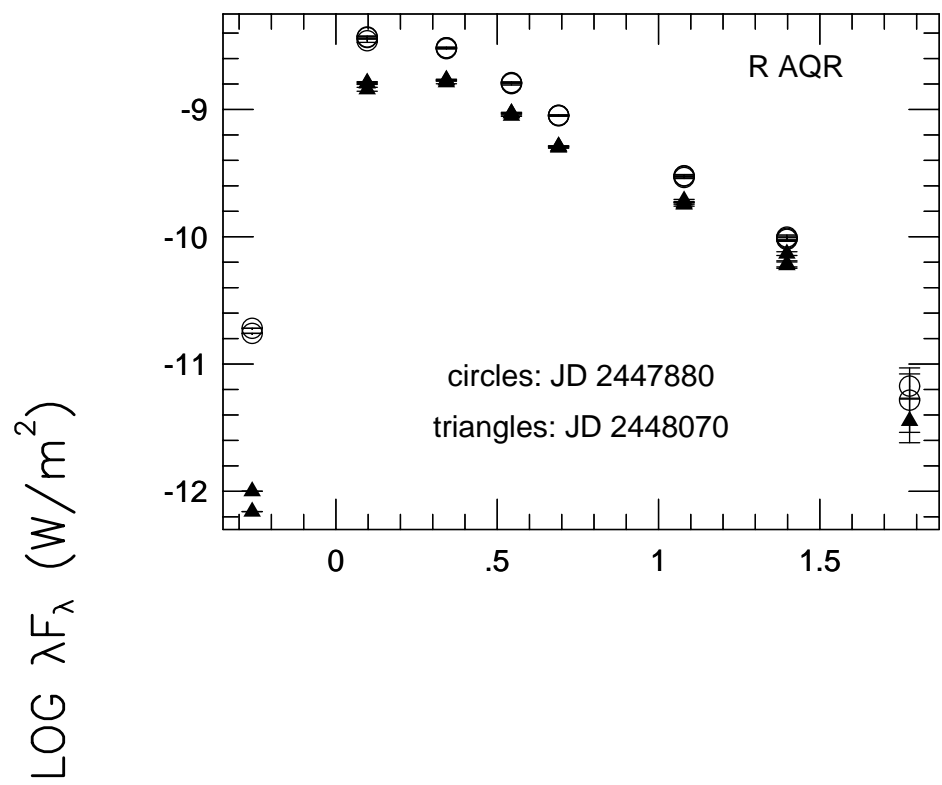
LOG WAVELENGTH (μm)



LOG WAVELENGTH (μm)

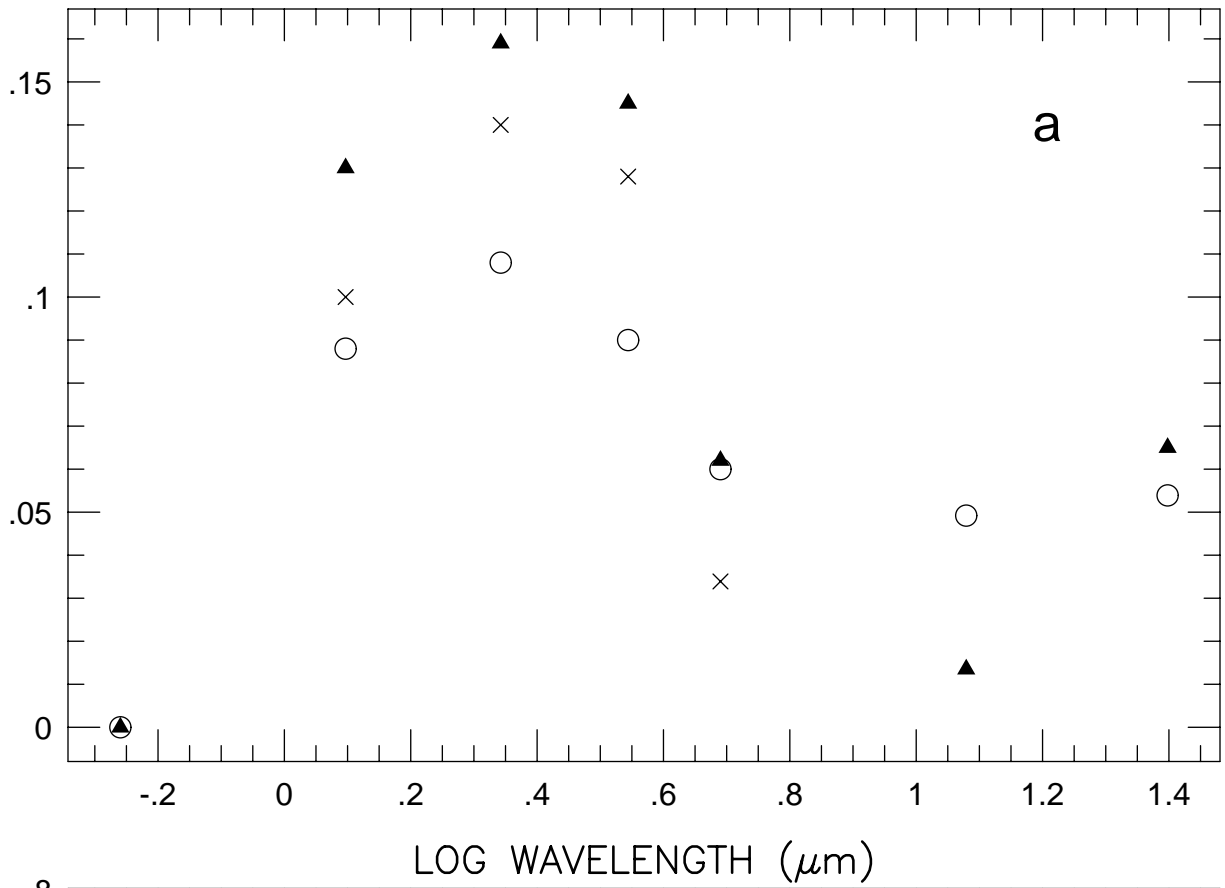


LOG WAVELENGTH (μm)



LOG WAVELENGTH (μm)

PHASE LAG RELATIVE TO V



AMPLITUDE

